Received: 21 February 2018 | Revised: 13 August 2018 | Accepted: 10 October 2018
DOI: 10.1002/gj.3368

RESEARCH ARTICLE

WILEY

The syncollisional granitoid magmatism and crust growth during the West Qinling Orogeny, China: Insights from the Jiaochangba pluton

Juanjuan Kong[1,2,3] | Yaoling Niu[1,2,4,5] | Meng Duan[5] | Fengli Shao[1,2,3] | Yuanyuan Xiao[1,2] | Yu Zhang[2] | Pengyuan Guo[1,2] | Pu Sun[1,2,3] | Hongmei Gong[1,2]

[1] Institute of Oceanology, Chinese Academy of Sciences, Qingdao, China
[2] Laboratory for Marine Geology, Qingdao National Laboratory for Marine Science and Technology, Qingdao, China
[3] University of Chinese Academy of Sciences, Beijing, China
[4] Department of Earth Sciences, Durham University, Durham, UK
[5] School of Earth Science and Resources, China University of Geosciences, Beijing, China

Correspondence
Juanjuan Kong, Institute of Oceanology, Chinese Academy of Sciences, Qingdao 266071, China.
Email: juanjuan0317@foxmail.com

Professor Yaoling Niu, Department of Earth Sciences, Durham University, Durham DH1 3LE, UK.
Email: yaoling.niu@durham.ac.uk

Funding information
Qingdao National Laboratory, Grant/Award Numbers: U1606401 and 2015ASKJ03; NSFC, Grant/Award Numbers: 41130314 and 41630968

Handling Editor: Erdin Bozkurt

The West Qinling Orogenic Belt (WQOB) is a major portion of the Qinling-Dabie-Sulu Orogen and holds essential information for understanding the protracted evolution of the north-eastern branch of the Paleo-Tethys in East Asia. In this study, we report our petrological, geochemical, and geochronological study on the five Triassic granitoid plutons of West Qinling with emphasis on the poorly studied Jiaochangba pluton with zircon U–Pb ages of 217.5 ± 1.6 Ma and 215.2 ± 1.2 Ma. The new data and the existing data on the other four plutons support the view that the West Qinling granitoids represent a magmatic response to the continental collision of the Yangtze Block (YB) with the North China Craton (NCC) in the Triassic. Like the other four plutons, the Jiaochangba pluton shows strong light rare earth element (REE) enrichment and weak heavy REE depletion ($[La/Sm]_N \approx 7.14 \pm 1.89$; $[Sm/Yb]_N \approx 4.63 \pm 1.85$) with varying negative Eu anomalies ($Eu/Eu^* \approx 0.65 \pm 0.20$). In the N-MORB normalized diagram, all the samples show relative enrichment in Rb, Pb, U, and K with negative Nb, Ta, P, and Ti anomalies, resembling those of the model continental crust. The Jiaochangba pluton has relatively lower $(^{87}Sr/^{86}Sr)_i$ (0.7062 to 0.7081), higher $\varepsilon_{Nd}(t)$ (−6.91 to −2.09), and $\varepsilon_{Hf}(t)$ (−5.57 to −0.14) than mature continental crust, which are consistent with their source being dominated by lower crust with significant mantle contributions. Mantle-derived melt, which formed from partial melting of mantle wedge peridotite facilitated by dehydration of the subducted/subducting Mianlue ocean crust, provide the required heat for the crustal melting while also contributing to the compositions of these granitoids. Evolution of such parental magmas in open system crustal magma chambers with continued evolution/replenishment and crustal contamination and assimilation give rise to the observed petrological and geochemical characteristics of these granitoids.

KEYWORDS
continental collision, Jiaochangba granitoids, lower crust melting, petrogenesis, West Qinling

1 | INTRODUCTION

It has been accepted that the bulk continental crust (BCC) has grown progressively through episodic magmatism over Earth's history (Condie, 2000). Granites are the most abundant igneous rocks in the Earth's upper continental crust. Hence, granitic magmatism has been widely used to study continental crust growth. Traditionally, continental crust is considered to be formed through subduction-zone magmatism because of the arc-like chemical signature of the BCC (e.g., enrichment of large-ion lithophile elements [LILEs], depletion in high-field-strength

© 2018 John Wiley & Sons, Ltd.

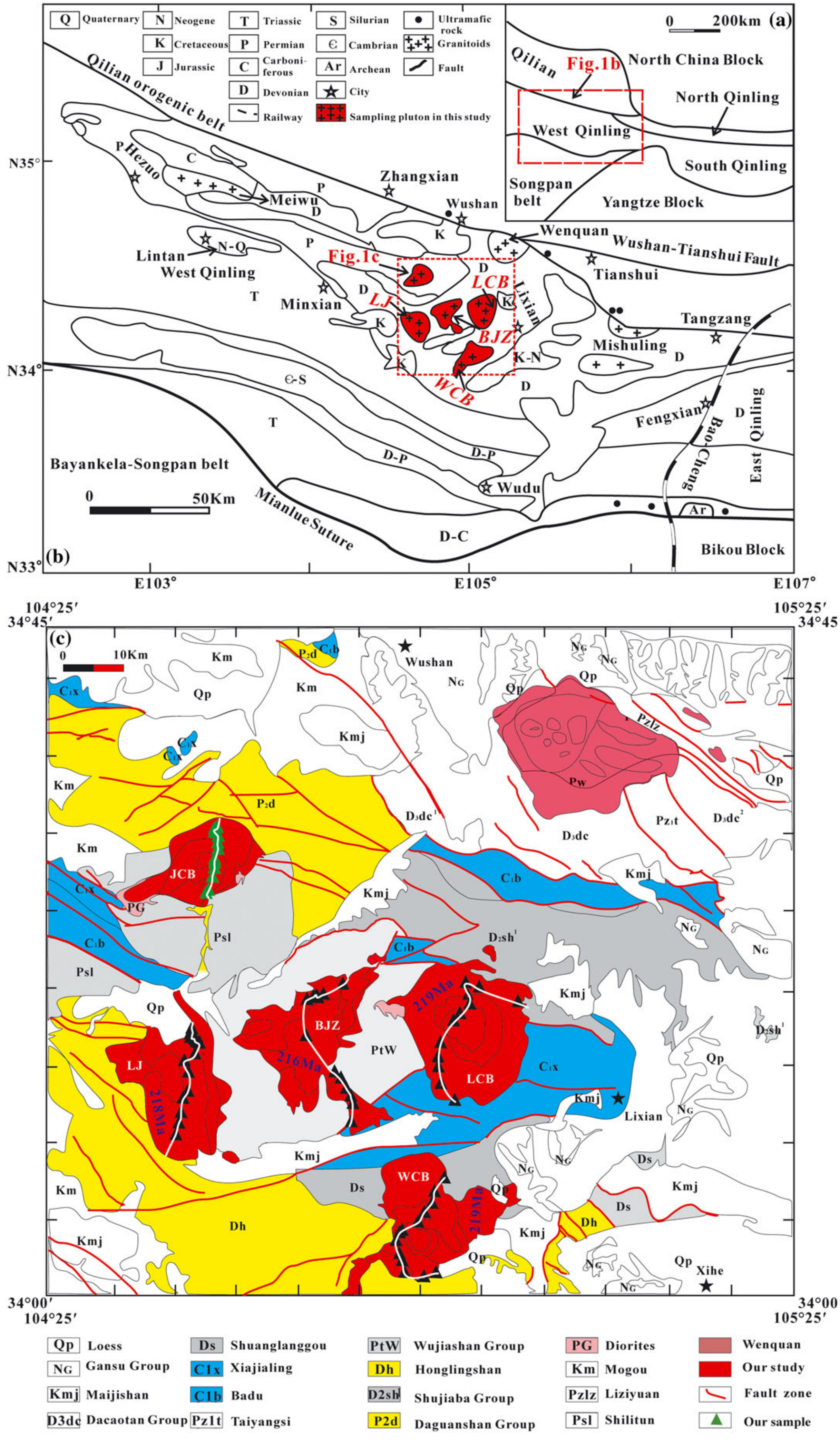

FIGURE 1 (a,b) Simplified geological map of the Western Qinling Orogenic belt (modified from Zhang et al., 2007). (c) Modified from 1:250,000 geological map of Minxian and Tianshui sheets (Xiao, 2004). The abbreviations are as follows: JCB = Jiaochangba, LCB = Luchuba, WCB = Wuchaba, LJ = Lvjing, BJZ = Baijiazhuang [Colour figure can be viewed at wileyonlinelibrary.com]

elements [HFSEs]), which is termed "island arc model" (Taylor, 1967). However, the "island arc model" has more difficulties than certainties, including, for example, (a) bulk arc crust is too mafic for the andesitic bulk continental crust; (b) arc settings have no net crustal addition (see Niu & O'Hara, 2009; Niu, Zhao, Zhu, & Mo, 2013). Because of this and on the basis of their detailed studies of the Linzizong syncollisional volcanic sequence in southern Tibet (Mo et al., 2008; Niu et al., 2007), Niu and co-workers (2013) hypothesize that continental collision zones are primary sites of net continental crustal growth. In this hypothesis, during continental collision, the remaining subducted ocean crust undergoes partial melting under amphibolite facies conditions, which produces and preserves granitoid magmas, contributing to net growth of continental crust. Because globally, active seafloor subduction is continuous, but continental collision is episodic, this hypothesis also satisfies the episodic growth of the continental crust and overcomes the difficulties of "island arc model." This hypothesis has been tested with success along several orogenic belts on the greater Tibetan Plateau (Chen et al., 2015; Huang et al., 2014; Mo et al., 2007; Mo et al., 2008; Niu & O'Hara, 2009; Niu et al., 2013; Shao et al., 2017; Zhang et al., 2016).

The Qinling Orogen developed through a series of complex seafloor subduction and terrene collision events (Dong et al., 2015; Ratschbacher et al., 2003; Wang et al., 2009; Wu & Zheng, 2012; Zhang, Zhang, Yuan, & Xiao, 2001), ultimately completed as a result of the continental collision of the Yangtze Block (YB) with the North China Craton (NCC) along the Mianlue suture zone in the Triassic (see Figure 1; Dong et al., 2011, and references therein). Abundant granitoids were produced in West Qinling this time and have received much attention in recent decades with mounting geochronological and geochemical data with the aim of better understanding magma sources and processes in the context of studying the Qinling orogenesis. However, the petrogenesis of these granitoids remains controversial, for example, magma mixing of mantle-derived basaltic magmas and crust-derived felsic magmas, upper crust melting or lower crust melting (e.g., Dong et al., 2012, 2011; Jiang, Jin, Liao, Zhou, & Zhao, 2010; Liang, Zhang, Bai, Jin, & Nantasin, 2015; Li, Liang, Zhang, Jiang, & Wang, 2017; Liu, Li, et al., 2011; Liu, Yang, et al., 2011; Peng, 2013; Qin et al., 2009, 2010; Sun, Li, Chen, & Li, 2002; Xiao et al., 2014; Yang et al., 2012, 2011; Zhu, Zhang, Yang, Wang, & Gong, 2013).

In this paper, we further test this hypothesis on syncollisional granitoids in the West Qinling Orogenic Belt (WQOB) by (1) presenting new LA-ICP-MS zircon U–Pb ages, whole-rock major and trace element data, and Sr–Nd–Hf isotopic compositions for the syncollisional Jiaochangba (JCB) pluton and (2) discussing the petrogenesis of the JCB granitoid pluton together with the four other coexisting granitoid plutons in space and time (i.e., Luchuba, Wuchaba, Lvjing, Baijiazhuang, and JCB).

2 | GEOLOGICAL SETTING AND SAMPLING

The Qinling Orogen has been divided into East and West Qinling on the basis of their geology (Zhang et al., 2007, 2001; Zhang, Zhang,

TABLE 1 Summary of lithologies, geochemistry, and geochronology of the five granitoid plutons in the West Qinling

		Geochemistry					Geochronology		
Locations	Lithology	A/CNK	Magmatic series	I_{Sr}	$\varepsilon_{Nd}(t)$	$\varepsilon_{Hf}(t)$	Age	Dating methods	References
Luchuba	Granodiorite and monzogranite	0.92–1.13	High-K calc-alkaline series	0.7051 to 0.7104	−8.11 to −4.58	−6.70 to −1.65	219 Ma	LA-ICP-MS zircon U–Pb	Kong et al., 2017
Wuchaba	Granodiorite and monzogranite	0.97–1.14	High-K calc-alkaline series	0.7072 to 0.7080	−9.86 to −5.52	−5.69 to −1.71	219 Ma	LA-ICP-MS zircon U–Pb	Kong et al., 2017
	MMEs	0.79–0.81	High-K calc-alkaline series	0.7069 to 0.7073	−4.74 to −3.34	−0.78 to 1.58			Kong et al., 2017
Lvjing	Granodiorite and monzogranite	0.99–1.12	High-K calc-alkaline series	0.7070 to 0.7080	−5.37 to −4.58	−0.36 to −1.78	218 Ma	LA-ICP-MS zircon U–Pb	Duan et al., 2016
	MMEs	0.81–0.88	High-K calc-alkaline series	0.7069 to 0.7161	−4.53 to −3.93	−1.38 to 2.37			Duan et al., 2016
Baijiazhuang	Granodiorite and monzogranite	0.92–1.22	High-K calc-alkaline series	0.7032 to 0.7078	−10.99 to −8.54	−10.22 to −6.41	216 Ma	LA-ICP-MS zircon U–Pb	Duan et al., 2016
JCB	Granodiorite and monzogranite	0.95–1.15	High-K calc-alkaline series	0.7062 to 0.7081	−6.91 to −3.97	−5.57 to −1.71	215 Ma	LA-ICP-MS zircon U–Pb	This study

Yan, & Wang, 2005; Feng et al., 2002). The WQOB is the western segment of the Qinling orogenic belt in central China, which is one of the largest in Asia (Mattauer et al., 1985), linking Kunlun and Qilian orogens to the west and Dabie-Sulu Orogen to the east (Lai & Zhang, 1996; Meng & Zhang, 2000; Ratschbacher et al., 2003). The west Qinling orogenic belt is adjacent to the Qilian orogenic belt (Figure 1 a) and is bounded by the Wushan-Tianshui Fault to the north and the Mianlue Suture to the south (Figure 1b). The granitoids are mainly of Indosinian age distributed along the north of the Mianlue Suture (Zhu et al., 2011). In the WQOB, the Phanerozoic stratigraphy is dominated by the Devonian-Cretaceous sedimentary sequences with minor Cambrian-Silurian sedimentary series (Feng et al., 2002). The JCB pluton located in the centre of the WQOB is circular in shape and covers ~120 km^2 in area and intruded the Permian strata (Figure 1c). We collected samples from the JCB pluton (104°37′31.0″–104°38′29.0″E, 34°26′21.3″–34°30′35.4″N) and its surrounding plutons (i.e., Luchuba, Wuchaba, Lvjing and Baijiazhuang; Figure 1 c). The Luchuba, Wuchaba, Lvjing, and Baijiazhuang plutons nearly all comprise diorites, quartz diorites, granodiorites, and monzogranites with varying amount of mafic magmatic enclaves (MMEs; Duan et al., 2016; Kong et al., 2017; Yang et al., 2017). The lithology, geochemistry, geochronology, and general characteristics of the five granitoid plutons including JCB pluton are given in Table 1.

The granitoid samples from the JCB pluton are intermediate- to coarse-grained biotite granites with grey to pink colours and granitic texture (Figure 2a). Their mineralogy includes K-feldspar (~20%), plagioclase (~35%), quartz (~30%), and minor hornblende and biotite (~5%) with accessory apatite, zircon, and Fe–Ti oxides (Figure 2c). Fine-grained mafic magmatic enclaves (MMEs) are dispersed in the JCB pluton (Figure 2b). The MMEs are of fine-grained granitic texture dominated by hornblende + biotite (~40% in total), plagioclase (~40%), and quartz (~15%) with accessory minerals similar to those in their granitoid host (Figure 2d). Figure 2d shows the sharp contact of MMEs with their host granodiorite, where MMEs are finer-grained than the host and have no chilled margins and textures of crystal resorption and reactive overgrowth. Mafic minerals and plagioclase are generally euhedral to subhedral, indicating that they may represent early-formed phases (see Reid & Hamilton, 1987), some plagioclase crystals showing clear zoning with K-feldspar and quartz being interstitial.

3 | ANALYTICAL METHODS

Ten freshest and representative samples from the JCB pluton were analysed for whole-rock major and trace elements and Sr–Nd–Hf isotope compositions. Two of the samples were selected for zircon U–Pb dating. Weathered surfaces and pen saw marks were removed and thoroughly cleaned, then ultrasonically cleaned with Milli-Q water and dried before powdered using an agate mill into ~200-mesh in a clean environment.

3.1 | LA-ICP-MS zircon U–Pb dating

Zircons were extracted using combined techniques of heavy liquid and magnetic separation. The zircon internal structure was examined using cathodoluminescence (CL) imaging on an EMPA-JXA-8100 scanning

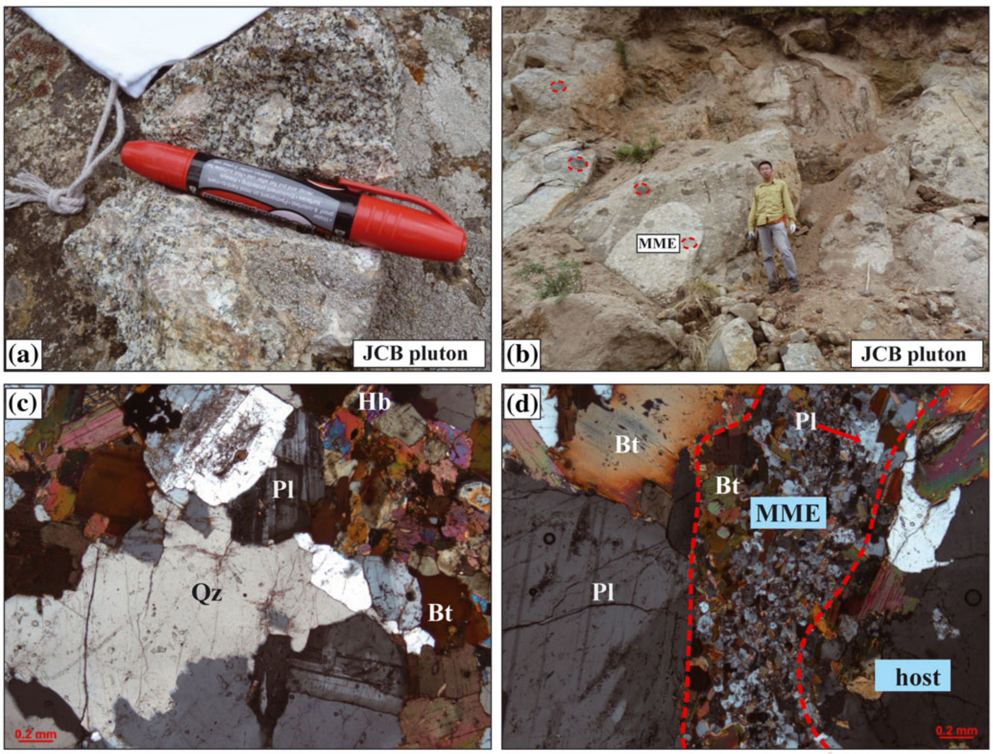

FIGURE 2 (a,b) An outcrop of JCB granitoid pluton with mafic magmatic enclaves (MMEs). (c) Photomicrographs of the JCB granitoid host (cross-polarized light or XPL) (d) Photomicrographs of the JCB MME (XPL). Showing the same mineralogy between the host granodiorite and their MMEs and the MMEs have greater mafic mineral modes. The abbreviations are as follows: Pl = Plagioclase, Qz = Quartz, Bt = Biotite, Hb = Hornblende [Colour figure can be viewed at wileyonlinelibrary.com]

electron microscope at China University of Geosciences, Wuhan (CUGW). Zircon U–Pb dating on samples JCB12-07 and JCB12-12 was carried out at the Geological Lab Center, China University of Geosciences, Beijing (CUGB) using an Agilent 7500a inductively coupled plasma mass spectrometry (ICP-MS) with a New Wave UPP-193 laser ablation system. During the analysis, laser spot size was set to ~36 μm for most analyses and to 25 μm for some rims, laser energy density at 8.5 J/cm^2 and repetition rate at 10 Hz. The procedure of laser sampling is 5-s pre-ablation, 20-s sample-chamber flushing, and 40-s sample ablation. The ablated material is carried into the ICP-MS by the high-purity Helium gas stream with flux of 0.8 L/min. The whole laser path was fluxed with N_2 (15 L/min) and Ar (1.15 L/min) in order to increase energy stability. Calibrations were done using NIST 610 glass as an external standard and Si as an internal standard.

TABLE 2 Zircon U–Pb data for the Jiaochangba pluton

	Th	U	Th/U	Corrected ratios				Corrected ages (Ma)			
				^{207}Pb/^{235}U	1σ	^{206}Pb/^{238}U	1σ	^{207}Pb/^{235}U	1σ	^{206}Pb/^{238}U	1σ
JCB12-07											
JC7-01	469	1205	0.39	0.26389	0.0053	0.0343	0.00049	238	4	217	3
JC7-02	92	473	0.19	0.23755	0.0068	0.03437	0.00051	216	6	218	3
JC7-03	188	288	0.65	0.23988	0.0078	0.03424	0.00053	218	6	217	3
JC7-04	163	838	0.19	0.26198	0.0073	0.03413	0.00049	236	6	216	3
JC7-05	344	1658	0.21	0.25685	0.0052	0.03435	0.00049	232	4	218	3
JC7-06	212	696	0.31	0.23909	0.0057	0.03426	0.0005	218	5	217	3
JC7-07	299	1871	0.16	0.24135	0.0054	0.03449	0.0005	220	4	219	3
JC7-08	460	1130	0.41	0.24898	0.0059	0.03448	0.0005	226	5	219	3
JC7-09	388	1269	0.31	0.24059	0.0055	0.0343	0.00049	219	4	217	3
JC7-10	85	110	0.78	0.23658	0.0091	0.03408	0.00055	216	7	216	3
JC7-11	356	451	0.79	0.23631	0.0062	0.03428	0.00052	215	5	217	3
JC7-12	1240	1134	1.09	0.23931	0.0074	0.03441	0.00052	218	6	218	3
JC7-13	554	3319	0.17	0.2493	0.005	0.03432	0.00049	226	4	218	3
JCB12-12											
JC12-01	465	914	0.51	0.23314	0.0099	0.03392	0.00052	213	8	215	3
JC12-02	117	420	0.28	0.23726	0.0091	0.03396	0.00051	216	7	215	3
JC12-03	260	1409	0.18	0.23621	0.005	0.03378	0.00049	215	4	214	3
JC12-04	327	934	0.35	0.24939	0.0085	0.0339	0.00051	226	7	215	3
JC12-05	258	956	0.27	0.23843	0.0077	0.03366	0.00049	217	6	213	3
JC12-06	347	1003	0.35	0.23797	0.0088	0.03397	0.00051	217	7	215	3
JC12-07	567	1346	0.42	0.2519	0.0057	0.03392	0.0005	228	5	215	3
JC12-08	314	1279	0.25	0.24173	0.0055	0.03423	0.0005	220	5	217	3
JC12-09	307	1028	0.30	0.23731	0.0084	0.03377	0.0005	216	7	214	3
JC12-10	229	818	0.28	0.24722	0.009	0.03385	0.00051	224	7	215	3
JC12-11	134	218	0.61	0.2349	0.0116	0.03388	0.00061	214	10	215	4
JC12-12	569	691	0.82	0.23655	0.0063	0.03401	0.00051	216	5	216	3
JC12-13	400	1157	0.35	0.24028	0.0055	0.03387	0.0005	219	5	215	3
JC12-14	459	1099	0.42	0.24085	0.0058	0.0339	0.0005	219	5	215	3
JC12-15	395	1125	0.35	0.255	0.0062	0.03471	0.00052	231	5	220	3
JC12-16	94	485	0.19	0.2368	0.0083	0.03384	0.00054	216	7	215	3
JC12-17	392	699	0.56	0.24843	0.007	0.0338	0.00052	225	6	214	3
JC12-18	332	296	1.12	0.23729	0.01	0.03389	0.00057	216	8	215	4
JC12-19	189	823	0.23	0.23776	0.0064	0.03402	0.00052	217	5	216	3
JC12-20	268	880	0.30	0.25994	0.0062	0.0338	0.0005	235	5	214	3
JC12-21	288	969	0.30	0.24577	0.0061	0.03393	0.00051	223	5	215	3
JC12-22	179	771	0.23	0.24116	0.0063	0.03385	0.00051	219	5	215	3
JC12-23	273	881	0.31	0.24447	0.006	0.03402	0.0005	222	5	216	3
JC12-24	403	939	0.43	0.23939	0.0059	0.03393	0.0005	218	5	215	3
JC12-25	278	1032	0.27	0.23446	0.0056	0.0339	0.0005	214	5	215	3
JC12-26	182	523	0.35	0.24877	0.0077	0.03382	0.00052	226	6	214	3
JC12-27	328	563	0.58	0.23576	0.0067	0.03386	0.00051	215	5	215	3

U–Pb isotope fractionation effects were corrected for using zircon 91500 (Wiedenbeck et al., 1995) as an external standard. The age data processed using the GLITTER4.41 program are given in Table 2 with analytical details given in Song, Niu, et al. (2010). The concordia diagrams and weighted mean age calculation were performed using ISOPLOT 4.15 (Ludwig, 2012; Figure 3).

3.2 | Mineral compositions

Mineral chemistry was determined using a JEOL EPMA8230 microprobe at Langfang, China. The operating conditions were 15 kV accelerating potential, probe current of 10 nA, and beam diameter of 1 μm. The analytical procedure follows the quantitative analysis of silicate minerals by electron probe microanalysis of the State Standard of the People's Republic of China (GB/T 15617-2002).

3.3 | Major and trace elements

Whole-rock major and trace elements were analysed using Prodigy Inductively Coupled Plasma Optical Emission Spectrometer (ICP-OES) and Agilent 7500a ICP-MS at CUGB, respectively. Analyses of United States Geological Survey (USGS) rock standards (AGV-2) and Chinese national rock standard (GSR-1 and GSR-3) give precisions (1σ) better than 1% for most major elements, except for TiO_2 (~1.5%) and P_2O_5 (~2%), and better than 5% for most trace elements. Analytical details are given in Song, Su, et al. (2010).

3.4 | Sr–Nd–Hf isotopes

The whole-rock Sr–Nd–Hf isotopic compositions of five samples were determined at CUGW following the chemical separation and analysis procedures of Gao et al. (2004) and Yang, Zhang, Chu, Xie, and Wu (2010). The Sr, Nd isotopic analyses were done on a Thermo Finnigan Triton Ti Thermal Ionization Mass Spectrometer (TIMS). The Hf isotopic analysis was done using a Thermo Neptune Plus Multi-Collector Inductively Coupled Plasma Mass Spectrometer (MC-ICP-MS). The other five samples for Sr–Nd–Hf isotopes were analysed using MC-ICP-MS in the Institute of Oceanology, Chinese Academy of Sciences (IOCAS), Qingdao. The chemical separation procedures are given in Sun et al. (2018) in preparation. Analysis of NBS987 standard run during the same period gave $^{87}Sr/^{86}Sr$ = 0.710254 ± 13 (n = 5, 2σ) and $^{143}Nd/^{144}Nd$ = 0.512109 ± 6 (n = 9, 2σ) for JNdi-1 standard. The Alfa Hf international standard yielded a mean $^{176}Hf/^{177}Hf$ of 0.282194 ± 11 (n = 13, 2σ). The values of USGS reference materials AGV-2, GSP-2, and RGM-2 run with our samples are given in

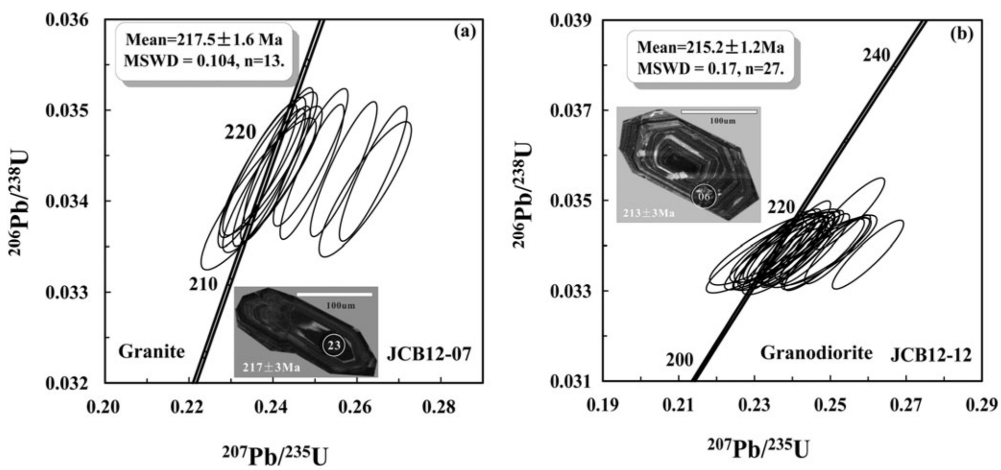

FIGURE 3 Zircon U–Pb concordia plots and weighted mean $^{206}Pb/^{238}U$ ages for (a) JCB12-07 and (b) JCB12-12 of the JCB pluton

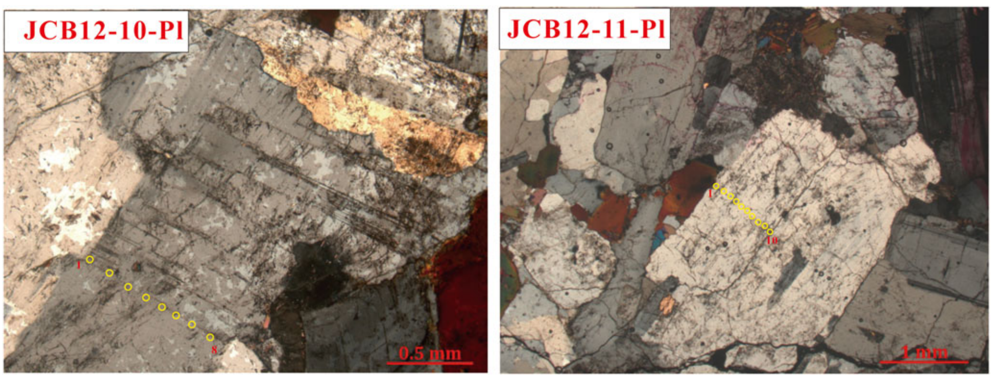

FIGURE 4 Plagioclase composition in granitoid hosts (JCB12-10) and the MME (JCB12-11). See Table 3a for compositional data [Colour figure can be viewed at wileyonlinelibrary.com]

TABLE 3 Microprobe analysis of plagioclase in the host granitoids and the mafic magmatic enclaves and microprobe analysis of amphibole in the host granitoids and the mafic magmatic enclaves

Spot	SiO_2	Al_2O_3	CaO	Na_2O	K_2O	Total	Si	Al	Ca	Na	K	An
JCB12–10-Pl												
1	61.62	24.72	5.86	8.25	0.20	100.74	2.72	1.29	0.28	0.71	0.01	28
2	61.71	24.59	5.78	8.38	0.32	100.85	2.72	1.28	0.27	0.72	0.02	27
3	62.07	23.85	5.06	8.62	0.23	99.97	2.76	1.25	0.24	0.74	0.01	24
4	60.90	24.60	6.10	8.22	0.25	100.19	2.71	1.29	0.29	0.71	0.01	29
5	61.00	24.21	5.70	8.47	0.26	99.76	2.72	1.27	0.27	0.73	0.02	27
6	60.80	24.69	5.98	8.20	0.22	100.02	2.71	1.30	0.29	0.71	0.01	28
7	60.83	25.19	6.34	8.20	0.30	101.05	2.69	1.31	0.30	0.70	0.02	29
8	61.83	24.68	6.01	7.78	0.23	100.56	2.73	1.28	0.28	0.67	0.01	30
9	61.52	24.06	5.55	8.40	0.46	100.21	2.73	1.26	0.26	0.72	0.03	26
10	60.56	24.93	6.36	7.95	0.30	100.27	2.69	1.31	0.30	0.69	0.02	30
JCB12–10-Pl												
1.1	62.69	24.07	5.25	8.78	0.24	101.12	2.75	1.25	0.25	0.75	0.01	25
1.2	60.48	24.82	5.83	8.14	0.23	99.58	2.70	1.31	0.28	0.70	0.01	28
1.3	55.66	27.50	9.29	6.10	0.13	98.76	2.53	1.47	0.45	0.54	0.01	45
1.4	60.71	24.65	6.12	8.14	0.20	99.84	2.70	1.29	0.29	0.70	0.01	29
1.5	60.75	24.57	6.11	8.25	0.30	100.06	2.70	1.29	0.29	0.71	0.02	29
1.6	61.02	24.59	5.82	8.12	0.23	99.90	2.72	1.29	0.28	0.70	0.01	28
1.7	60.70	24.98	6.37	7.91	0.21	100.28	2.69	1.31	0.30	0.68	0.01	30
1.8	61.35	25.10	6.23	8.36	0.18	101.28	2.70	1.30	0.29	0.71	0.01	29
JCB12–11-Pl												
1.1	61.91	23.61	5.04	8.79	0.17	99.64	2.76	1.24	0.24	0.76	0.01	24
1.2	60.05	24.90	6.24	8.06	0.17	99.56	2.69	1.31	0.30	0.70	0.01	30
1.3	56.46	27.41	9.22	6.23	0.09	99.52	2.55	1.46	0.45	0.55	0.01	45
1.4	59.62	25.28	6.91	7.62	0.10	99.65	2.67	1.33	0.33	0.66	0.01	33
1.5	56.15	27.88	9.66	6.10	0.12	99.98	2.52	1.48	0.47	0.53	0.01	46
1.6	55.66	27.43	9.42	6.22	0.16	98.98	2.53	1.47	0.46	0.55	0.01	45
1.7	61.59	24.70	6.14	8.19	0.16	100.84	2.72	1.28	0.29	0.70	0.01	29
1.8	61.14	24.62	5.89	8.01	0.28	100.14	2.72	1.29	0.28	0.69	0.02	28
1.9	60.75	24.93	6.33	8.15	0.22	100.53	2.69	1.30	0.30	0.70	0.01	30
1.10	62.09	23.75	4.85	9.10	0.10	100.10	2.76	1.24	0.23	0.78	0.01	23
JCB12–11-Pl-a												
1.1	60.87	24.49	5.81	8.36	0.30	100.03	2.71	1.29	0.28	0.72	0.02	27
1.2	59.19	25.55	7.13	7.62	0.15	99.79	2.65	1.35	0.34	0.66	0.01	34
1.3	58.57	26.08	7.50	7.25	0.13	99.66	2.63	1.38	0.36	0.63	0.01	36
1.4	58.05	26.21	7.79	7.26	0.15	99.59	2.61	1.39	0.38	0.63	0.01	37
1.5	58.80	25.73	7.20	7.47	0.15	99.52	2.64	1.36	0.35	0.65	0.01	34
1.6	57.59	26.29	8.24	6.82	0.18	99.20	2.60	1.40	0.40	0.60	0.01	40
1.7	58.09	26.67	8.07	6.95	0.13	99.99	2.60	1.41	0.39	0.60	0.01	39
1.8	58.89	25.78	7.20	7.57	0.11	99.68	2.64	1.36	0.35	0.66	0.01	34
1.9	61.09	24.28	5.61	8.51	0.10	99.71	2.72	1.28	0.27	0.74	0.01	27

Spot	SiO_2	TiO_2	Al_2O_3	NiO	FeO	MnO	Cr_2O_3	MgO	CaO	Na_2O	K_2O	Total
JCB12–10-Amp												
1.1	49.09	0.48	3.84	0.00	18.89	0.55	0.05	10.87	11.39	0.64	0.35	96.14
1.2	48.07	0.68	4.83	0.03	18.98	0.60	0.00	10.55	11.10	0.92	0.44	96.20
1.3	45.27	1.21	6.79	0.02	19.40	0.56	0.01	9.12	11.25	1.05	0.67	95.34
1.4	49.88	0.50	4.07	0.03	18.22	0.49	0.05	10.83	11.93	0.57	0.32	96.88
1.5	47.84	0.72	5.18	0.07	18.99	0.50	0.04	10.18	11.64	0.52	0.46	96.14
1.6	48.25	0.75	4.90	0.05	18.72	0.59	0.03	10.42	11.30	0.81	0.46	96.27

(Continues)

TABLE 3 (Continued)

Spot	SiO_2	TiO_2	Al_2O_3	NiO	FeO	MnO	Cr_2O_3	MgO	CaO	Na_2O	K_2O	Total
1.7	47.96	0.75	4.73	0.02	17.89	0.55	0.02	10.62	10.75	0.74	0.39	94.41
1.8	44.97	1.26	7.51	0.00	19.48	0.57	0.02	8.92	10.85	1.28	0.84	95.70
Si	**Ti**	**Al**	**Al**	**Cr^{3+}**	**Fe^{3+}**	**Fe^{2+}**	**Mg**	**Mn**	**Ca**	**Na**	**K**	**Mg#**
7.42	0.05	0.58	0.11	0.01	0.27	2.12	2.45	0.07	1.85	0.08	0.07	0.54
7.29	0.08	0.71	0.15	0.00	0.26	2.13	2.38	0.08	1.80	0.11	0.08	0.53
7.00	0.14	1.00	0.24	0.00	0.18	2.33	2.10	0.06	1.86	0.07	0.13	0.47
7.49	0.06	0.51	0.21	0.01	0.05	2.24	2.42	0.04	1.92	0.04	0.06	0.52
7.26	0.08	0.74	0.19	0.00	0.26	2.15	2.30	0.05	1.89	0.06	0.09	0.52
7.31	0.09	0.69	0.19	0.00	0.18	2.20	2.35	0.08	1.84	0.09	0.09	0.52
7.37	0.09	0.64	0.22	0.00	0.19	2.07	2.43	0.07	1.77	0.12	0.08	0.54
6.94	0.15	1.06	0.31	0.00	0.13	2.37	2.05	0.07	1.79	0.11	0.17	0.46
Spot	**SiO_2**	**TiO_2**	**Al_2O_3**	**NiO**	**FeO**	**MnO**	**Cr_2O_3**	**MgO**	**CaO**	**Na_2O**	**K_2O**	**Total**
JCB12–11-Amp												
1.1	50.58	0.15	3.09	0.00	17.22	0.44	0.04	11.93	11.62	0.48	0.19	95.74
1.2	50.89	0.20	3.08	0.00	17.15	0.47	0.02	12.03	11.70	0.55	0.19	96.26
1.3	50.95	0.25	2.95	0.03	18.17	0.47	0.00	11.86	11.57	0.62	0.17	97.03
1.4	51.23	0.22	2.88	0.01	16.58	0.47	0.02	12.79	11.60	0.55	0.23	96.56
1.5	50.21	0.50	3.55	0.01	17.06	0.46	0.02	12.33	11.44	0.74	0.28	96.59
1.6	50.15	0.60	3.37	0.04	17.86	0.58	0.03	12.11	10.96	0.75	0.32	96.76
1.7	48.59	1.09	4.69	0.00	18.31	0.58	0.01	11.50	10.65	0.92	0.38	96.72
1.8	50.23	0.52	3.86	0.03	17.11	0.51	0.04	11.95	11.41	0.52	0.33	96.52
Si	**Ti**	**Al**	**Al**	**Cr^{3+}**	**Fe^{3+}**	**Fe^{2+}**	**Mg**	**Mn**	**Ca**	**Na**	**K**	**Mg#**
7.60	0.02	0.40	0.15	0.01	0.18	1.98	2.67	0.06	1.87	0.07	0.04	0.57
7.61	0.02	0.39	0.15	0.00	0.14	2.01	2.68	0.06	1.87	0.07	0.04	0.57
7.58	0.03	0.42	0.10	0.00	0.23	2.02	2.63	0.06	1.84	0.08	0.03	0.57
7.60	0.02	0.40	0.10	0.00	0.21	1.83	2.83	0.06	1.84	0.08	0.04	0.61
7.48	0.06	0.52	0.10	0.00	0.23	1.88	2.74	0.06	1.83	0.09	0.05	0.59
7.47	0.07	0.53	0.06	0.00	0.32	1.86	2.69	0.07	1.75	0.13	0.06	0.59
7.26	0.12	0.74	0.09	0.00	0.37	1.85	2.56	0.07	1.71	0.16	0.07	0.58
7.49	0.06	0.51	0.17	0.00	0.20	1.92	2.66	0.06	1.82	0.09	0.06	0.58

Appendix A, which are consistent with the recommended reference values (GeoREM, http://georem.mpch-mainz.gwdg.de/).

4 | RESULTS

4.1 | Zircon U–Pb age

Zircon grains from the JCB pluton are ~100 to 300 μm in size and have a length/width ratio of 1:1 to 3:1 (Figure 3a,b). They have clear oscillatory zoning in the CL images and display varying U (110 to 3319 ppm) and Th (85 to 1240 ppm) with Th/U ratios of 0.16 to 1.12, which are consistent with being of magmatic origin (Corfu, Hanchar, Hoskin, & Kinny, 2003; Hanchar & Hoskin, 2003; Rubatto & Gebauer, 2000). Thirteen zircon grains of JCB12-07 give apparent $^{206}Pb/^{238}U$ ages of 216 ± 3 Ma to 221 ± 3 Ma, with a weighted mean age of 217.5 ± 1.6 Ma (MSWD = 0.104, n = 13; Figure 3a). However, it is noteworthy that some data points plot to the right side of the concordia, probably due to analytical uncertainty of ^{207}Pb and trace common lead (Yuan et al., 2003). Twenty-seven zircons from sample JCB12-12 give a weighted mean $^{206}Pb/^{238}U$ age of 215.2 ± 1.2 Ma (MSWD = 0.17, n = 27; Figure 3b). These ages represent the emplacement age of the JCB pluton, which are in agreement with the time of the NCC-YB collision (Dong et al., 2012).

4.2 | Mineral compositions

Carefully selected plagioclase and amphibole crystals were analysed for major element composition using electron microprobe, in which Fe^{2+} and Fe^{3+} values of amphibole were recalculated after Lin and Peng (1994).

However, the lack of reversed zoning rules out the magma mixing hypothesis for the petrogenesis of the MMEs and their host granodiorite (Figure 4 and Table 3). Following Leake et al. (1997), amphiboles from the MMEs and their host granodiorite are compositionally the same and can be classified as calcic magnesiohornblende with high $Mg^{\#}$ (0.46–0.61) [$Mg^{\#} = Mg/(Mg + Fe^{2+})$] (Figure 5 and Table 3). All the amphibole crystals of the MMEs and their host granodiorite are compositionally uniform without zoning (Table 3). Moreover, the mafic minerals in the MME are richer in Mg and plagioclases are more calcic

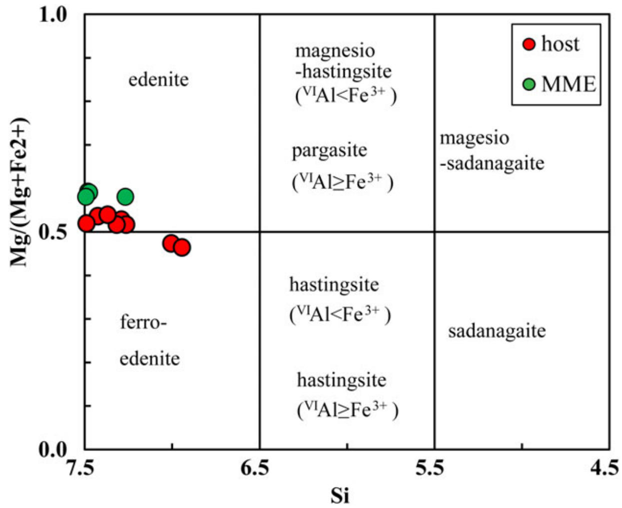

FIGURE 5 Chemical compositions of amphiboles from granitoid hosts (JCB12-10) and the MME (JCB12-11) in the amphibole classification diagram (Leake et al., 1997). See Table 3b for compositional data [Colour figure can be viewed at wileyonlinelibrary.com]

than those of the host (Table 3), support the mafic cumulate model for the MMEs (see Chen et al., 2016).

4.3 | Major and trace elements

The analytical data for whole-rock major and trace element compositions are given in Table 4. In the total alkalis-silica (TAS) diagram (Figure 6a), the granitoid host samples plot in the granite and granodiorite field and the MME samples plot in the granodiorite and gabbroic diorite field. The samples are compositionally high-K calc-alkaline with high K_2O/Na_2O (0.79–1.62 for the host and 1.52 for the MME; Figure 6b) and weak peraluminous to metaluminous with varying A/CNK (0.95–1.15 for the host and 0.62 for the MME; Figure 6c). On SiO_2-variation diagrams (Figure 7), the granitoids define inverse linear trends for major elements (e.g., TiO_2, Al_2O_3, TFe_2O_3, MgO, CaO, P_2O_5) and selected trace elements (Sr, Eu, and Zr), which are apparently consistent with fractionation of amphibole, biotite, and plagioclase and are more directly controlled by modal mineralogy of the samples. It should also be noted that in the majority of the silica variation diagrams (Figure 7), the JCB MME composition differs significantly from both the host rock and other MMEs compositions for its high mode of mafic minerals.

The JCB granitoid host samples display highly fractionated REE patterns $(La/Yb)_N$ = 3.86 to 48.51, [La/Sm]N > 1, [Sm/Yb]N > 1) and moderate negative Eu anomalies (Eu/Eu* = 0.30 to 0.85;i.e., weak HREEs depletion, Figure 8). The MME sample shows $(La/Yb)_N$ = 12.96 and Eu/Eu* = 0.80 (Figure 8). The Nb/Ta ratios (10.64 to 17.05 with an average of 14.79) of the host rocks and MME (14.95) are sub-chondritic (chondrite Nb/Ta ratio: 17.5; Sun & McDonough, 1989), even lower than that of upper oceanic crust (16.08; Niu & O'Hara, 2009). In the multi-element diagram, all the samples are enriched in LILEs (e.g., Rb, K, Pb) and relatively depleted in HFSEs (e.g., Nb, Ta, Ti; Figure 8b). These characteristics resemble those of bulk continental crust (BCC; Rudnick & Gao, 2003).

4.4 | Sr–Nd–Hf isotopes

Whole rock Sr–Nd–Hf isotope data for 10 samples (including MME) of the JCB pluton are given in Table 5 and plotted in Figures 9 and 12. The $I_{Sr}(t)$, $\varepsilon_{Nd}(t)$, and $\varepsilon_{Hf}(t)$—where t = 220 Ma—are variable, that is, $I_{Sr}(t)$ = 0.7062 to 0.7081, $\varepsilon_{Nd}(t)$ = −6.91 to −3.97, and $\varepsilon_{Hf}(t)$ = −5.57 to −1.71. The whole-rock Nd isotopic model ages (T_{DM}) are essentially the same (~1.2–2.3 Ga) as the two-stage Hf model ages (T_{DM2} ~1.0–2.0 Ga). The MME sample also shows similar Sr–Nd–Hf isotopic compositions ($I_{Sr}(t)$ = 0.7066, $\varepsilon_{Nd}(t)$ = −2.09, $\varepsilon_{Hf}(t)$ = −0.14) to the host granitoid sample. Sample JCB12-06 of the JCB pluton gives very high $^{87}Sr/^{86}Sr$ of 0.8681 because of the high Rb/Sr ratio ($^{87}Rb/^{86}Sr$ ~55.1) due to significant plagioclase-dominated fractional crystallization (also low in Ba, P, and Ti; see Figure 8b), resulting in high radiogenic ^{87}Sr ingrowth, which makes the calculated $I_{Sr}(t)$ unreliable (Jahn, Wu, & Chen, 2000).

5 | DISCUSSION

5.1 | Roles of Fractional Crystallization

As shown in the figures, the JCB granitoids display compositional variations. Apart from the effects of magma source heterogeneity and the extent of melting, crystal fractionation can be important factors contributing to the compositional variations. Therefore, it is necessary to evaluate the potential effect of the fractional crystallization before discussing source characteristics of the JCB granitoids.

As pointed out above, the JCB granitoids slightly decrease in TiO_2, Al_2O_3, TFe_2O_3, MgO, CaO, P_2O_5, Sr, and Eu with increasing SiO_2 (Figure 7), likely suggestive of fractional crystallization of ferromagnesian minerals (biotite ± hornblende), plagioclase, Fe–Ti oxides, and apatite (Rollison, 1993). The granitoids exhibit decreasing Zr with increasing SiO_2 (Figure 7), indicating that zircon was saturated and on the liquidus (Li et al., 2007; Zhong et al., 2009). Negative Eu anomalies and depleted Ti, P show that fractional crystallization of plagioclase, Fe–Ti oxides, and apatite is important in the petrogenesis (Figure 8). Positive correlations of CaO with Sr and Eu/Eu* (Figure 10a,b) are consistent with modal plagioclase control in the samples (resulting from either plagioclase accumulation or crystallization removal). Figure 11 shows that fractionation of K-feldspar, plagioclase, and biotite played an important role in the petrogenesis of the JCB granitoids. The granitoids show sub-chondritic Nb/Ta ratio (10.64 to 17.05 with an average of 14.79) and depleted in Nb, Ta in spider diagram resulting from the higher partition coefficient of Nb than Ta during hornblende crystallization ($Kd_{hornblende}$ Nb/Ta = 1.40; Foley, Tiepolo, & Vannucci, 2002). Therefore, fractional crystallization is important in the petrogenesis of these granitoids.

5.2 | Petrogenesis of the JCB pluton

Generally, granitoids are typically divided into I-, S-, A-, and M-type in terms of source rock types and petrogenesis (Chappell & White, 1974; Collins, Beams, White, & Chappell, 1982; Whalen, 1985). The samples of the JCB pluton have $(^{87}Sr/^{86}Sr)_i$ of 0.7062 to 0.7081, $\varepsilon_{Nd}(t)$ of −6.91

TABLE 4 Major (wt.%) and trace element concentrations (ppm) of the Jiaochangba pluton

	JCB12-01	JCB12-04	JCB12-06	JCB12-08	JCB12-09	JCB12-10	JCB12-11	JCB12-12	JCB12-15	JCB12-17
Major elements (wt.%)										
SiO_2	72.47	73.87	75.54	70.31	64.62	66.16	56.43	63.64	71.91	74.58
TiO_2	0.25	0.26	0.05	0.35	0.65	0.59	0.72	0.66	0.33	0.09
Al_2O_3	14.28	13.87	13.52	14.98	16.60	16.04	13.19	16.28	14.07	13.98
TFe_2O_3	1.41	1.65	0.45	2.38	4.39	4.24	8.02	4.43	1.83	0.81
MnO	0.03	0.04	0.02	0.05	0.07	0.07	0.25	0.07	0.05	0.03
MgO	0.40	0.49	0.09	0.78	1.63	1.69	6.58	1.65	0.54	0.19
CaO	0.96	1.35	0.56	2.10	3.46	3.51	6.94	3.49	1.30	0.80
Na_2O	3.36	3.77	3.30	3.79	4.18	3.93	2.63	3.87	3.67	3.56
K_2O	4.91	4.59	5.36	3.95	3.48	3.11	3.99	4.05	4.51	4.51
P_2O_5	0.13	0.08	<0.03	0.12	0.37	0.21	0.41	0.33	0.07	0.07
LOI	0.81	0.55	0.32	0.49	0.7	0.61	0.87	0.6	0.73	0.74
Total	99.01	100.52	99.21	99.30	100.16	100.16	100.05	99.07	99.02	99.35
A/CNK	1.04	0.97	0.98	1.04	1.04	1.06	0.68	0.99	1.01	1.06
K_2O/Na_2O	1.46	1.22	1.62	1.04	0.83	0.79	1.52	1.05	1.23	1.27
Trace elements (ppm)										
Li	127	111	35.8	90.1	66.5	44.5	33.2	112	114	83.5
P	289	171	46	446	981	723	1889	1292	383	121
K	47500	37020	57420	36640	32520	27420	48180	43200	41720	45620
Sc	2.64	1.80	1.16	4.06	6.92	5.72	32.6	8.06	3.57	3.10
Ti	1689	1559	388	2328	4528	3588	5590	5026	2190	537
V	16.7	18.6	4.37	38.5	86.5	63.2	292	93.9	20.6	10.6
Cr	12.3	5.30	2.62	10.8	29.9	18.6	287	28.5	28.3	4.30
Mn	275	308	136	435	615	425	2114	682	404	268
Co	1.50	2.22	0.39	4.59	10.4	7.71	28.5	10.7	2.61	0.35
Ni	6.04	1.86	1.59	4.65	15.8	7.50	37.8	11.2	13.4	1.62
Cu	2.48	2.52	—	4.86	14.6	10.0	101	15.1	1.62	17.8
Zn	50.7	56.2	41.6	45.1	75.9	57.3	104	74.8	51.0	28.9
Ga	24.7	20.9	21.2	19.9	23.4	19.5	17.7	22.5	23.2	22.9
Rb	299	224	527	188	145	123	113	141	309	319
Sr	180	135	28	320	563	486	373	550	204	88
Y	9.40	12.8	9.93	13.3	16.0	13.5	26.0	16.9	14.8	15.6
Zr	189	157	42.5	158	259	210	177	262	200	80.0
Nb	19.3	22.2	18.3	20.7	20.7	17.0	14.6	22.0	24.3	25.6
Cs	12.7	18.5	26.1	9.85	7.38	7.71	3.44	6.85	22.8	16.0
Ba	724	394	30	660	1271	999	1568	1501	565	244
La	47.8	29.4	6.65	20.5	51.3	39.4	40.6	45.8	33.6	19.7
Ce	92.1	55.7	13.8	46.2	105	73.7	90.1	90.6	66.9	40.1
Pr	9.13	6.05	1.55	4.60	10.1	7.65	11.5	9.38	6.89	4.20
Nd	30.4	21.3	5.9	17.5	36.4	27.1	47.2	33.3	24.1	14.9
Sm	4.90	4.09	1.50	3.82	6.36	4.86	9.59	6.03	4.49	3.52
Eu	0.748	0.501	0.164	0.899	1.55	1.25	2.35	1.50	0.68	0.34
Gd	3.39	3.24	1.42	3.29	5.12	3.90	8.04	4.84	3.55	3.11
Tb	0.384	0.428	0.249	0.443	0.622	0.484	0.985	0.616	0.474	0.474
Dy	1.81	2.30	1.59	2.37	3.12	2.50	5.11	3.13	2.60	2.66
Ho	0.311	0.424	0.330	0.436	0.556	0.437	0.943	0.558	0.477	0.502
Er	0.836	1.23	1.07	1.24	1.50	1.16	2.62	1.45	1.39	1.46
Tm	0.114	0.178	0.174	0.175	0.195	0.152	0.353	0.195	0.196	0.214
Yb	0.706	1.20	1.24	1.15	1.24	1.01	2.25	1.23	1.29	1.44
Lu	0.098	0.176	0.183	0.174	0.177	0.143	0.326	0.175	0.187	0.205
Hf	4.53	3.85	1.13	4.20	5.86	4.82	4.46	6.04	4.98	2.36

(Continues)

TABLE 4 (Continued)

	JCB12-01	JCB12-04	JCB12-06	JCB12-08	JCB12-09	JCB12-10	JCB12-11	JCB12-12	JCB12-15	JCB12-17
Ta	1.22	1.39	1.72	1.49	1.21	1.20	0.97	1.47	1.92	1.42
Pb	29.1	30.1	61.1	27.1	21.0	19.5	23.3	19.7	32.3	40.5
Th	28.7	21.2	10.0	17.2	15.8	12.9	7.4	14.3	23.6	15.2
U	1.91	2.91	1.21	3.03	4.91	1.95	5.14	3.19	3.49	8.71
Eu/Eu*	0.53	0.41	0.34	0.76	0.80	0.85	0.80	0.82	0.50	0.30
$(La/Yb)_N$	48.51	17.57	3.85	12.78	29.77	28.09	12.96	26.77	18.63	9.85

Note. A/CNK = molar $Al_2O_3/(CaO + Na_2O + K_2O)$; Eu/Eu* = W $(Eu)_N$/[(1/2) (W $(Sm)_N$ + W $(Gd)_N$)]; $(La/Yb)_N$ is normalized by Chondrite, Chondrite values are from Sun and McDonough (1989).

to −3.94, and $\varepsilon_{Hf}(t)$ of −5.57 to −2.66, have no aluminous minerals such as muscovite, tourmaline, and garnet, and have mafic mineral assemblage of hornblende and biotite (Figure 2). All these, plus relatively low A/CNK values (<=1.1; Figure 6c), are consistent with most of these granitoids being of I-type granitoid.

The earlier study proposed three models to explain the origin of the JCB granitoids pluton: (a) mixing of mafic and felsic magmas on the basis of Sr and O isotopes (Wen, 2008); (b) melting of upper crustal argillaceous rocks (Peng, 2013) by interpreting the trace element data; (c) Lower crust melting explained for the congenetic granitoids with JCB (Gao, 2011).

The JCB pluton contains MMEs. The origin of the MMEs is a key to the petrogenesis of the granitoids and has been the subject of debate (Barbarin, 2005; Chappell, White, Williams, Wyborn, & Wyborn, 2000; Yang, Wu, Wilde, & Liu, 2007; Niu et al., 2013; Huang et al., 2014; Chen et al., 2016, 2015). Here, we discuss the MMEs of the five syn-collision granitoid plutons (JCB, Luchuba, Wuchaba, Lvjing, and Baijiazhuang; see Figure 1; Duan et al., 2016; Kong et al., 2017). Several lines of evidence favouring the mafic cumulate model are addressed below: (a) the petrography shows typical magmatic textures (Figure 2d), ruling out the MMEs being of restite; (b) the MMEs do not show core-to-rim mineral compositional and textural variations, excluding MMEs being of metasomatic origin (Figure 2d) (Eberz & Nicholls, 1990); (c) the MMEs have the same minerals as the host granitoids but have higher modal amphibole (and biotite). Note that the MMEs have high Cr and Ni contents, consistent with high partition coefficients of Cr and Ni for amphibole and biotite (Ewart & Griffin, 1994); (d) the MMEs have the same age as their host (Jiang, 2016); (e) their different major and trace element abundances from their hosts are largely controlled by mineral modal proportions (Figures 7 and 8); (f) MMEs have slightly higher $\varepsilon_{Nd}(t)$, $\varepsilon_{Hf}(t)$ than their host granitoids and similar $(^{87}Sr/^{86}Sr)_i$ (Figure 9). Obviously, the data are more consistent with the same mantle source with varying extents of crustal contamination (Figure 9a,b,c). The MMEs are less contaminated because they are earlier cumulate whereas the remaining magma continues to evolve and assimilate with the crustal country lithologies before solidified as the granitoid hosts. This is a straightforward geological process (Chen et al., 2015; Niu et al., 2013). It is worthy to note that the bulk composition of the JCB-MME sample is gabbroic diorite (lack of pyroxene), which is different from the granodioritic compositions of other MMEs because of it contains more hornblende. Importantly, the MMEs comprise dominantly amphibole and plagioclase (Figure 2d), which are common cumulate minerals in andesitic melts. If the parental melts were basaltic, the typical cumulate from such evolved basaltic melt would be gabbro dominated by clinopyroxene and plagioclase. This is an important petrological concept. It is worth to note that the same or very similar observations mentioned above have been commonly used as evidence for magma mixing for MME-bearing granitoids. Many researchers (e.g., Pin, Binon, Belin, Barbarin, & Clemens, 1990; Holden, Halliday, & Stephens, 1987; Poli & Tommasini, 1991; Elburg, 1996) have claimed partial or complete isotopic equilibration of the MMEs with their host. Experiments show that the isotopic equilibration advances faster than the chemical equilibration and Sr isotopic equilibrium is faster than that of Nd (e.g., Holden et al., 1987; Pin et al., 1990). Someone holds that compared with the Nd, the Sr isotopic compositions of the host and enclaves are more likely to be equilibrated through diffusion exchange, but it is physically unlikely with isotopes being homogenized whereas major and trace elements are not. Therefore, we maintain that the MMEs are early cumulate as the host granitoids.

In the eastern segment of the south Qinling tectonic unit, there are widespread Precambrian basement exposures, for example, the Yudongzi Group, the Foping Group, the Douling Group, the Wudang Group, the Yaolinghe Group, and the Yunxi Group. Their formation time is from the Neoarchean, Paleoproterozoic to Neoproterozoic based on geochronology (Zhang, Zhang, & Tang, 2002). According to Nd isotopic compositional comparison between the WQOB granitoids and the Precambrian basements of the South Qinling, none of the basements can be taken as the magma source for the WQOB granitoids (Zhang et al., 2007). The JCB pluton has lower and constant $(^{87}Sr/^{86}Sr)_i$, higher $\varepsilon_{Nd}(t)$ and $\varepsilon_{Hf}(t)$ than the mature continental crust (upper crust; $[^{87}Sr/^{86}Sr]_i$ < 0.72, $\varepsilon_{Nd}(t)$ > −12; the reference data are from Niu & O'Hara, 2009). Obviously, it is unlikely that these granitoids were produced by melting mature continental crust (upper crust) but has significant mantle contribution (or juvenile continental crust) in terms of isotopes. In addition, the slightly radiogenic Hf–Nd isotopes are coupled and lie in the global mantle and crustal array (Figure 9d) and removed far away from (higher than) mature continental crust, which is again consistent with mantle input, reflecting the process of juvenile continental crust formation manifested by the petrogenesis of these granitoids. Some studies suggest that amphibolite dehydration of lower crust can produce such magmas (Zhang et al., 2007), yet amphibolite melting preferentially produces high-Na_2O, not high-K_2O magmas, which are different from the JCB granitoids (Figure 6 b; Beard & Lofgren, 1991). Moreover, the chondrite-normalized REE patterns (Figure 8a) contradicts with the geochemical signatures formed by partial melting of lower crustal garnet amphibolite or

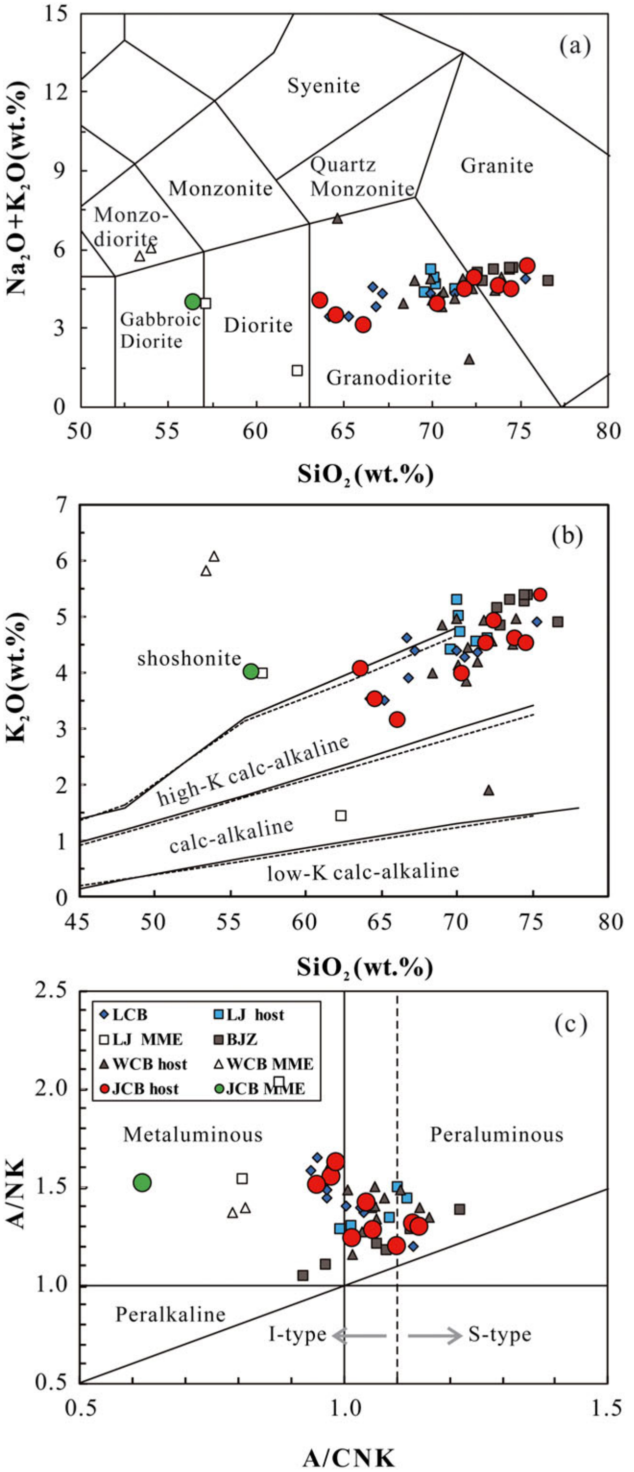

FIGURE 6 (a) Total alkalis ($Na_2O + K_2O$) versus SiO_2 (TAS) diagram showing the compositional variation of the JCB samples. The MME is less felsic than the granitic hosts. (b) Diagram of K_2O vs. SiO_2 for granitoids of JCB pluton. (c) Diagram of A/NK [$Al_2O_3/(Na_2O + K_2O)$] vs. A/CNK [molar ratio $Al_2O_3/(CaO + Na_2O + K_2O)$] for granitoids of JCB pluton [Colour figure can be viewed at wileyonlinelibrary.com]

eclogite. Thus, the origin by only partial melting of the pre-existing lower crust is unlikely.

To produce such andesitic to felsic BCC-like magmas with inherited mantle-like isotopic composition, it requires a basaltic source plus continental materials. The "island arc" model can produce the "continental signature" (e.g., enriched in LREEs and LILEs, depleted in HFSEs) and mantle-like isotopes. However, the bulk arc crust is too mafic to produce the more felsic melts (Niu et al., 2013). Although Lee and Anderson (2015) offered a solution to this difficulty, partial melting of arc crust will produce high Sr magmas, yet the Sr of the JCB plutons is not as high as island arc basalts (IAB), but only slightly higher than MORB (Niu & O'Hara, 2009) The plagioclase separation can lead to low Sr but it cannot reduce the high Sr/Sr* values in IAB (see fig. 4 in Niu et al., 2013). Thus, this model is inadequate to explain the JCB pluton in the WQOB. When the palaeogeographic evolution is taken into account, the sedimentary facies change from turbiditic deposits during the Early-Middle Triassic to shallow marine–terrestrial deposits during the Middle-Late Triassic in WQOB (Yan, Wang, Li, Xu, & Deng, 2012). Furthermore, the lack of Late Triassic sedimentary rocks in the South Qinling belt suggests that the Mianlue oceanic basin has been closed during the Late Triassic (Yang et al., 2012). Therefore, the Late Triassic (~210–220 Ma) magmatism witnessed a period of continental collision. In addition, Mo et al. (2008) already demonstrate that syncollisional magmatism is capable to produce volumetrically significant I-type granitoid plutons. Therefore, we suggest the JCB pluton formed in a syncollisional setting. The popular explanation is that a thermal pulse associated with slab breakoff resulted in the asthenosphere upwelling along the Mianlue Suture during the Late Triassic, and the upwelling asthenosphere triggered partial melting of the Neoproterozoic sub-continental lithosphere mantle (SCLM) that generated the mafic magma and the partial melting of the Neo-Mesoproterozoic lower crust that generated the granitic magmatism (Qin et al., 2009; Yang et al., 2015; Zhu et al., 2013). As noted above, only lower crust melting is unlikely to produce the observed granitoids, and the MMEs as the magmatic cumulate of hornblende-plagioclase assemblage cannot represent mafic magma of SCLM origin, because the asthenosphere mantle cannot upwell and melt upper crust to generate granitic magmas (Wen, 2008) without complete lithosphere removal (delamination). Importantly, the popular slab-breakoff model in explaining syncollisional magmatism is physically unlikely (Niu, 2017). Therefore, this interpretation for mixing of mafic and felsic magmas is unlikely to generate the JCB pluton in dynamics.

In this case, a reasonable mechanism in a syncollisional setting proposed by Niu et al. (2013) is possibly effective in explaining the petrogenesis of these granitoids. Partial melting of subducted basaltic ocean crust under the amphibolite facies conditions can produce andesitic melts with inherited mantle isotopic signatures (Niu et al., 2013). Partial melting of oceanic crust cannot generate high K/Na melts, and crust contribution is necessary. Isotopes also require possible contributions of continental crustal materials (see above). The host granitoids and the MME have indistinguishable Sr isotopic compositions and $\varepsilon_{Nd}(t)$ and $\varepsilon_{Hf}(t)$ correlated with SiO_2 (Figure 9a,b,c), manifesting significant crustal contamination of these granitoids. The $\varepsilon_{Nd}(t)$ and $\varepsilon_{Hf}(t)$ and SiO_2 of MMEs of JCB, Luchuba, Wuchaba, Lvjing, and Baijiazhuang are weakly positively correlated, suggesting the contamination of cumulate samples (MMEs) after their separation from the main body of largely liquid magma (parent magmas) (Reiners, Nelson, & Nelson, 1996), which accords with the cumulate origin of the MMEs (see above). Crustal assimilation with concurrent fractional crystallization (AFC) is now widely considered as an important process

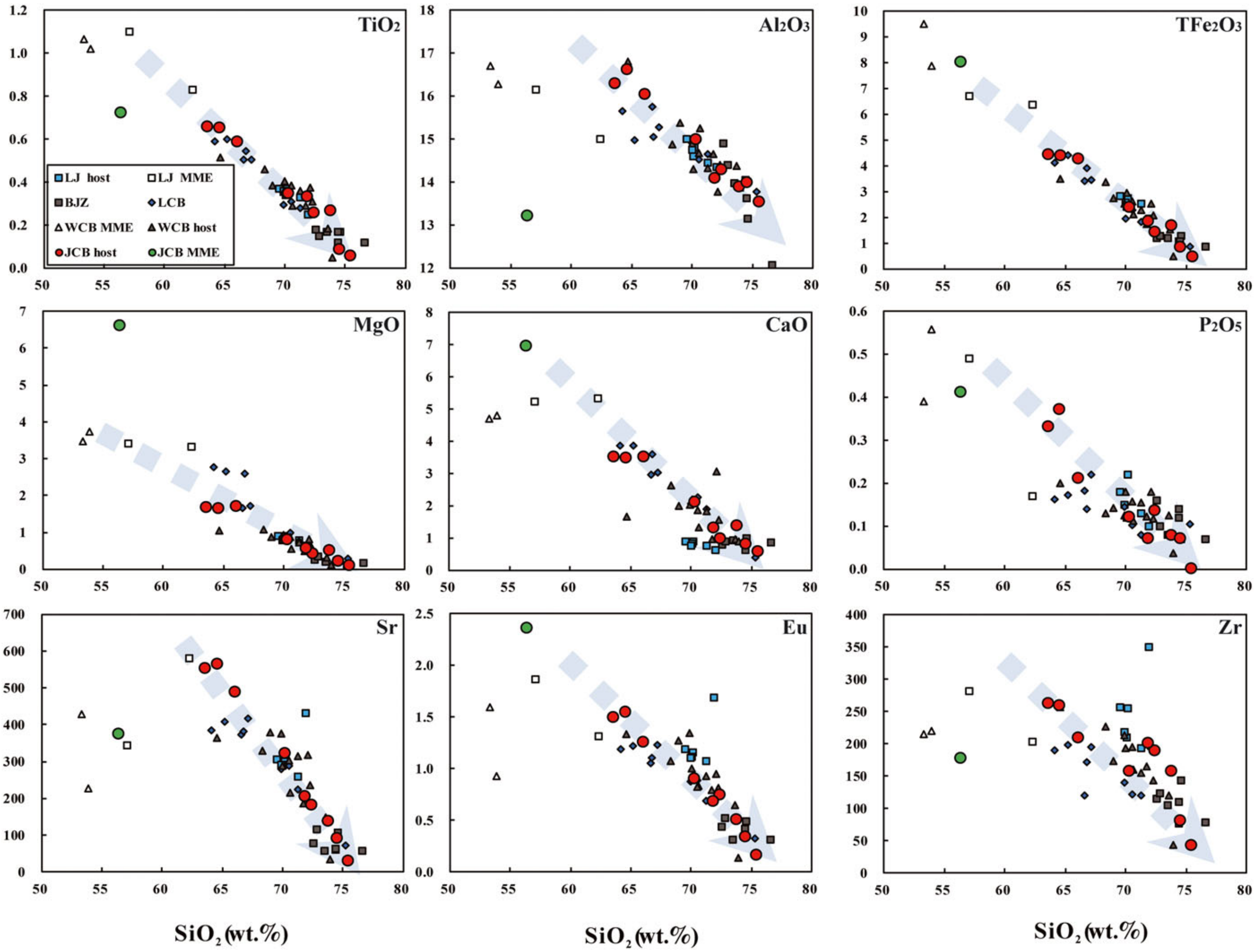

FIGURE 7 SiO_2 variation diagrams of representative major element oxides (wt.%) and selected trace elements (ppm) of the JCB samples [Colour figure can be viewed at wileyonlinelibrary.com]

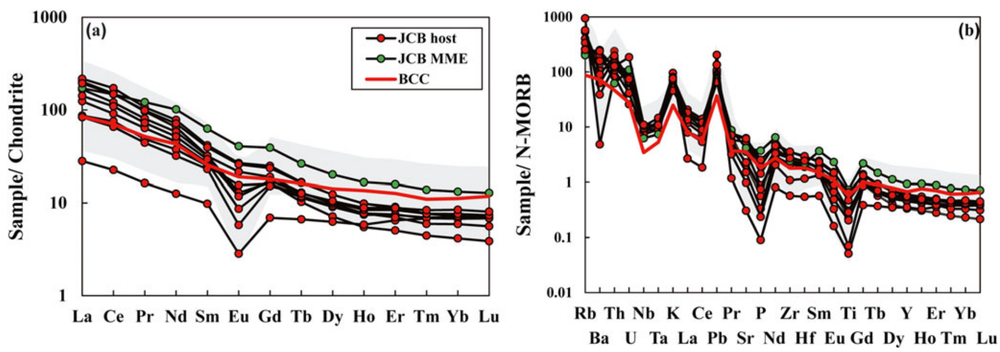

FIGURE 8 (a) Chondrite-normalized REE patterns, and (b) N-MORB normalized incompatible element abundances of samples from the JCB pluton; For comparison, the average Bulk continental crust (BCC, red solid line) (Rudnick & Gao, 2003) is also plotted. Chondrite and N-MORB values are from Sun and McDonough (1989). The data of shades of grey are from Duan et al. (2016); Kong et al. (2017) [Colour figure can be viewed at wileyonlinelibrary.com]

of magma evolution (Depaolo, 1981). AFC or fractional crystallization (FC) of basaltic magma can produce granitoids (Bowen, 1928). These suggest that the AFC from parental magmas of basaltic or more likely mafic andesitic compositions may be a suitable mechanism for the JCB granitoids. Hence, partial melting of subducted basaltic ocean crust under the amphibolite facies in combination with magma evolution through AFC processes can explain the petrogenesis of the JCB pluton. But simple isotopic calculations show only ~40–45% ocean crust (MORB) contribution (the maximum contribution) to the source of these granitoids (Figure 12). In the calculation, the Mianlue oceanic crust slab is represented by the 350 Ma ophiolitic MORB in Qinling, central China (Xu et al., 2002), and upper crust is represented by the average composition of ~2000 Ma Douling gneiss in South Qinling (Shen et al., 1997). 55–60% mature continental crust contribution

TABLE 5 Sr, Nd, Hf isotopes of the Jiaochangba pluton

Sample	$^{87}Rb/^{86}Sr$	$^{87}Sr/^{86}Sr$	±2σ	$(^{87}Sr/^{86}Sr)_i$	$^{147}Sm/^{144}Nd$	$^{143}Nd/^{144}Nd$	±2σ	$\varepsilon_{Nd}(t)$	T_{DM} (Ga)	$^{176}Lu/^{177}Hf$	$^{176}Hf/^{177}Hf$	±2σ	$\varepsilon_{Hf}(t)$	T_{DM2} (Ga)
JCB12-01	4.787	0.723015	0.000004	0.708062	0.098	0.512142	0.000002	−6.91	1.3	0.003	0.282491	0.000003	−5.57	1.6
JCB12-04	4.783	0.722216	0.000004	0.707272	0.117	0.512221	0.000003	−5.90	1.5	0.006	0.282554	0.000002	−3.83	1.6
JCB12-06	55.1	0.868100	0.000007	0.696051	0.155	0.512276	0.000003	−5.89	2.3	0.023	0.282655	0.000003	−2.65	2.5
JCB12-08	1.696	0.711905	0.000004	0.706605	0.133	0.512329	0.000003	−4.25	1.5	0.006	0.282598	0.000002	−2.17	1.5
JCB12-09	0.741	0.708909	0.000004	0.706594	0.106	0.512293	0.000004	−4.19	1.2	0.004	0.282573	0.000002	−2.83	1.5
JCB12-10	0.730	0.708917	0.000005	0.706636	0.109	0.512309	0.000003	−3.97	1.2	0.004	0.282578	0.000002	−2.66	1.5
JCB12-11	0.871	0.709309	0.000005	0.706588	0.124	0.512426	0.000003	−2.09	1.2	0.010	0.282674	0.000002	−0.14	1.5
JCB12-12	0.740	0.709150	0.000005	0.706837	0.110	0.512302	0.000003	−4.14	1.2	0.004	0.282604	0.000002	−1.71	1.4
JCB12-15	4.363	0.720885	0.000004	0.707253	0.113	0.512214	0.000004	−5.94	1.4	0.005	0.282560	0.000002	−3.44	1.5
JCB12-17	10.4	0.738834	0.000007	0.706214	0.143	0.512217	0.000003	−6.71	2.0	0.012	0.282540	0.000003	−5.19	1.9

Note. t = crystallization time of zircon (~220 Ma). $^{87}Rb/^{86}Sr$, $^{147}Sm/^{144}Nd$, $^{176}Lu/^{177}Hf$ ratios calculated using Rb, Sr, Sm and Nd contents, measured by ICP-MS. $(^{147}Sm/^{144}Nd)_{CHUR} = 0.1967$, $(^{143}Nd/^{144}Nd)_{CHUR} = 0.512638$; $(^{176}Lu/^{177}Hf)_{CHUR} = 0.0332$, $(^{176}Hf/^{177}Hf)_{CHUR} = 0.282772$ (Blichert-Toft et al., 1997); $(^{147}Sm/^{144}Nd)_{DM} = 0.2137$, $(^{143}Nd/^{144}Nd)_{DM} = 0.51315$; $(^{176}Lu/^{177}Hf)_{DM} = 0.0384$, $(^{176}Hf/^{177}Hf)_{DM} = 0.28325$ (Griffin et al., 2002) was used in the calculations. JCB12-01,09,10,11,17 are analysed in CUGW, JCB12-04,06,08,12,15 are analysed in IOCAS.

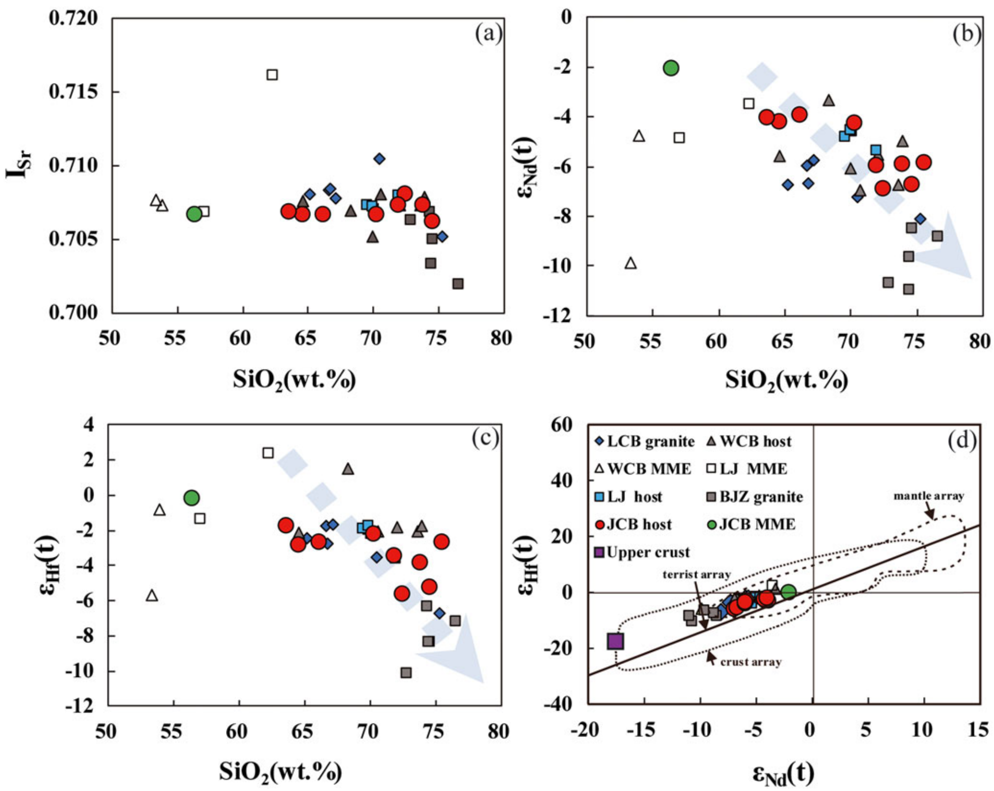

FIGURE 9 (a)-(c) Plots of Sr, Nd and Hf isotopes (in the forms of initial $^{87}Sr/^{86}Sr$ or I_{Sr}, $\varepsilon_{Nd}(t)$ and $\varepsilon_{Hf}(t)$) against SiO_2, showing isotopes between MMEs with lower SiO_2 and the host granitoids with higher SiO_2. The data of LJ, BJZ from Duan et al. (2016) and the data of WCB, LCB from Kong et al. (2017). (d) The $\varepsilon_{Nd}(t)$ of upper crust (mature crust) is from Reiners, Nelson, and Ghiorso (1995) and the $\varepsilon_{Hf}(t)$ is inferred from Nd isotope following the equation ($\varepsilon_{Hf} = 1.59\varepsilon_{Nd} + 1.28$) given by (Chauvel, Lewin, Carpentier, Arndt, & Marini, 2008). The field for crust–mantle array is from Vervoort, Patchett, Blichert-Toft, and Albarède (1999) and the terrestrial array is from Vervoort, Plank, and Prytulak (2011) [Colour figure can be viewed at wileyonlinelibrary.com]

likely means the melting occurred at crust depth. MORB melting model cannot reasonably explain the petrogenesis of JCB granitoids. The whole-rock Nd isotopic model ages (T_{DM}; 1.2–2.3 Ga) and two-stage Hf model ages (T_{DM}; 1.0–2.0 Ga) of JCB granitoids support a source composed of ancient lower continental crust (Qin et al., 2009). Therefore, we propose a more reasonable model that is consistent with the observations and basic petrological concepts. When the Mianlue oceanic slab subducted beneath the Qinling Block, dehydration of the ocean crust can effectively lower the solidus of mantle wedge peridotite to melt for the basaltic melt (e.g., Pearce & Peate, 1995). Extraction, ascent, and underplating of such mantle wedge-derived basaltic melts can induce the lower continental crustal melting to produce magmas parental to the JCB granitoids (Figure 13). All these processes are likely taking place in an open system with

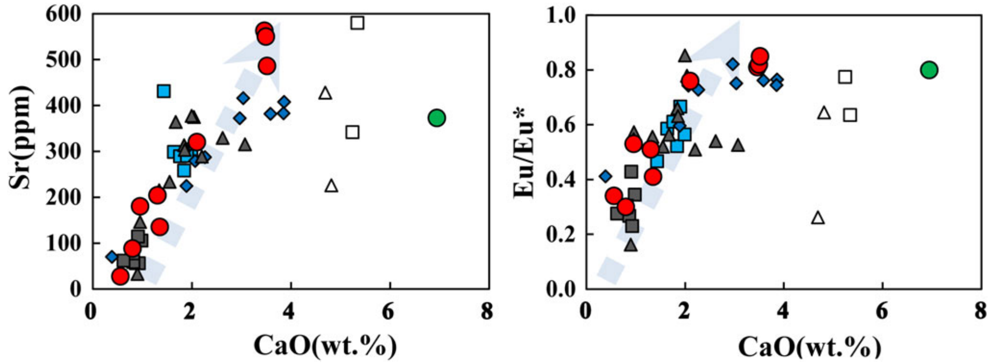

FIGURE 10 (a) CaO versus Eu/Eu* diagram; (b) CaO versus Sr diagram. The graphic symbol as Figure 5 [Colour figure can be viewed at wileyonlinelibrary.com]

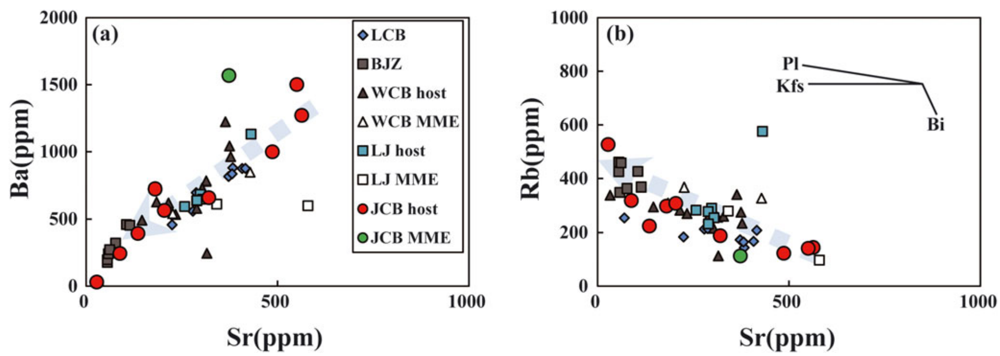

FIGURE 11 (a) Sr versus Ba diagram; (b) Sr versus Rb diagram [Colour figure can be viewed at wileyonlinelibrary.com]

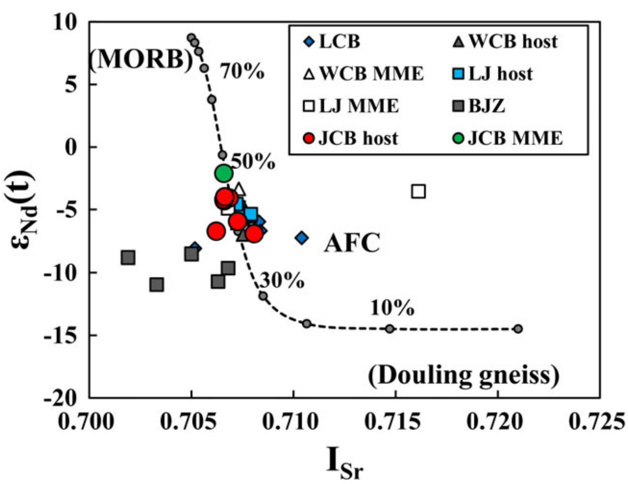

FIGURE 12 Plot of $^{87}Sr/^{86}Sr$ vs. $\varepsilon_{Nd}(t)$ for JCB granitoids. The modelled AFC path uses parental magma (Mianlue MORB) with 93 ppm Sr (I_{Sr}: 0.705), 6.5 ppm Nd ($\varepsilon_{Nd}(t)$: 8.71) (Xu, Castillo, Li, Zhang, & Han, 2002) and a hypothetical basement rock Douling gneiss from south Qinling with 268 ppm Sr (I_{Sr}: 0.721) and 26 ppm Nd ($\varepsilon_{Nd}(t)$: −14.5) (Shen, Zhang, & Liu, 1997) for conceptual simplicity. AFC path calculated according to (DePaolo et al., 1981) equation. The ratio of assimilation to fractionation was set at r = 0.15. Bulk Kd's for Sr and Nd were 0.36 and 0.86, respectively [Colour figure can be viewed at wileyonlinelibrary.com]

continued evolution/replenishment accompanied by crustal contamination and assimilation. Such mantle-derived melt also contributes materials to the granitoid magmatism, that is, there exists mixing between the mantle-derived isotopically depleted melt and isotopically enriched felsic melt from the lower continental crust, which is consistent with variable isotope compositions (Figure 9). Here, we emphasize that components from depleted mantle wedge and upper crust materials must have been involved in the formation process of the granitic magmas. When a primitive magma body is emplaced into a cold environment with the wall rock having temperatures below the liquidus of the magma, magma quench and rapid crystallization are inevitable because of the thermal contrast, despite the high viscosity of granitoids. The first major liquidus phases of parental magma of the granitoids would be amphibole, biotite, plagioclase, and rapid quench and will facilitate abundant nucleation without between-nuclei space for growth, thus forming fine-grained MME cumulate, which can be readily disturbed by replenishing magmas, leading to the dispersed MMEs (Chen et al., 2016, 2015) in the granitoid hosts.

5.3 | The origin of granitoids in West Qinling

All the five plutons (JCB, Luchuba, Wuchaba, Lvjing, and Baijiazhuang) are clustered together (Figure 1), which is commonly called "the Zhongchuan pluton group" in the WQOB (Peng, 2013). The genetic relationship of the five plutons remains poorly known (Li, Duan, & Li, 1993; Peng, 2013; Xu, M, & Wang, 2006). The JCB pluton and the other four syncollisional plutons (Luchuba, Wuchaba, Lvjing, and Baijiazhuang; Duan et al., 2016; Kong et al., 2017; Figure 1) have MMEs and show similar mineralogy

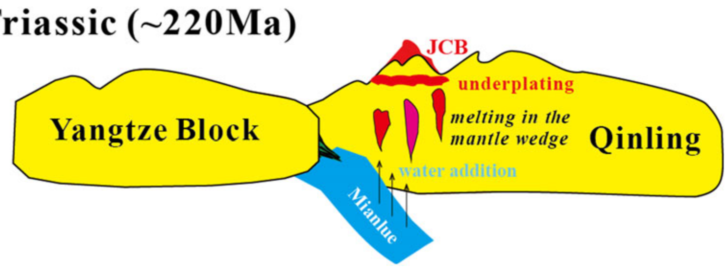

FIGURE 13 Schematic illustration for the generation of the JCB granitoids in West Qinling during the late Triassic (~220 Ma). See text for explanation [Colour figure can be viewed at wileyonlinelibrary.com]

(Qz + Pl + Kfs + Bt ± Hb ± Zircon ± Apatite ± Fe–Ti oxides) with varying modes. They are metaluminous to weakly peraluminous I-type or S-type granitoids and largely belong to high-K calc-alkaline series (Figure 6). These granitoids have similar REE patterns with LREEs enrichment, significant Eu anomalies and trace element patterns resembling those of BCC (Figure 8) and show the similar Sr–Nd–Hf isotope characters with inherited mantle-like isotopic signatures likely from the mantle wedge, the large Nd–Hf isotope ranges due to the magmas underwent various degrees crustal contamination. Importantly, they have the same intrusive ages (Table 1), all these indicating they are products of the same thermal and tectonic event.

5.4 | Significance of continental crust growth in the WQOB

In our study, trace element patterns of the JCB, Luchuba, Wuchaba, Lvjing, and Baijiazhuang plutons resemble those of BCC. Despite the more felsic and radiogenic Sr compositions of the five granitoid plutons, it has relatively higher $\varepsilon_{Nd}(t)$ and $\varepsilon_{Hf}(t)$ than that of mature continental crust ($[^{87}Sr/^{86}Sr]_i$ < 0.72, $\varepsilon_{Nd}(t)$ > −12; Niu & O'Hara, 2009). In particular, the value of $\varepsilon_{Nd}(t)$ and $\varepsilon_{Hf}(t)$ of these granitoids is obviously higher than the value of continental crust (see Figures 9d and 12), pointing to the contributions of mantle or juvenile crust materials (see Section 5.2). Hence, this syncollisional pluton represents juvenile crust with primary materials may come from the mantle wedge.

5.5 | Tectonic Significance

Our new data also give insights into the evolution of the Qinling Orogen. The detailed geochronological data for the high-pressure/ultrahigh-pressure (HP/UHP) metamorphic rocks manifested that the subduction and continental collision between the NCC and YB took place no later than ca. 230 Ma in the Dabie-Sulu Orogen (Liu, Xu, Liou, & Song, 2004; Zheng, 2008). In comparison, our studied granitoids in the Qinling region represent the initial stage of the NCC-YB continental collision after ~220 Ma, which were later than the continental collision age in the Dabie-Sulu Orogen (~230 Ma). Our results show that subduction of the Mianlue oceanic crust beneath the WQOB was still going on before ~220 Ma and the final closure of the Mianlue oceanic basin occurred at ~220 Ma. Considering the Paleo-Tethyan Mianlue oceanic basin between the NCC and the YB in the Dabie-Sulu Orogen closed ~10 Myrs is earlier than that in the Qinling Orogen.

6 | CONCLUSIONS

(1) Zircon U–Pb dating yields ages of 217.5 ± 1.6 Ma and 215.2 ± 1.2 Ma for the JCB pluton, essentially the same as the ages of other four plutons in the area. We interpret this magmatism as response to the collision of the Yangtze Block with the North China Craton.

(2) The granitoids of the JCB, Luchuba, Wuchaba, Lvjing, and Baijiazhuang plutons display an enriched LILEs and LREE pattern and have variably strong negative Eu anomalies, which is similar to those of bulk continental crust but more evolved. The enriched Sr–Nd–Hf isotope compositions suggest that their main source is the ancient lower continental crust. However, components from depleted mantle wedge and upper crust materials must have been involved in the petrogenesis of the granitic magmas.

(3) We suggest that oceanic crust slab dehydration-induced mantle wedge melting remains the primary mechanism for mantle-derived basaltic melts, whose underplating and intrusion of the crust can cause continental crustal melting.

(4) Jiaochangba, Luchuba, Wuchaba, Lvjing, and Baijiazhuang plutons are products of the same thermal and tectonic event.

ACKNOWLEDGEMENTS

The research is supported by NSFC (Grants 41130314, 41630968) and Qingdao National Laboratory (Grants U1606401, 2015ASKJ03). We thank Shuo Chen, Huixia Cui, Zhenxing Hu, Jiyong Li, Jinju Liu, Yuxin Ma, Wenli Sun, Xiaohong Wang, Lei Ye, Xiaolu Ye, and Guorui Zhang for assistance with sample preparation. We particularly thank Su Li for major and trace analysis and zircon analysis and Zhou Lian for Sr–Nd–Hf isotope analysis. We also thank Erdin Bozkurt and three anonymous reviewers for their constructive comments and suggestions on the manuscript improvement.

CONFLICT OF INTEREST

No potential conflict of interest was reported by the authors.

ORCID

Juanjuan Kong https://orcid.org/0000-0001-8698-3295

REFERENCES

Barbarin, B. (2005). Mafic magmatic enclaves and mafic rocks associated with some granitoids of the central Sierra Nevada batholith, California: Nature, origin, and relations with the hosts. *Lithos*, *80*, 155–177. https://doi.org/10.1016/j.lithos.2004.05.010

Beard, J. S., & Lofgren, G. E. (1991). Dehydration melting and water-saturated melting of basaltic and andesitic greenstones and amphibolites at 1, 3 and 6.9 kb. *Journal of Petrology*, *32*, 465–501.

Blichert-Toft, J., Chauvel, C., & Albarède, F. (1997). Separation of Hf and Lu for high-precision isotope analysis of rock samples by magnetic sector-multiple collector ICP-MS. *Contributions to Mineralogy and Petrology*, *127*(3), 248–260. https://doi.org/10.1007/s004100050278

Bowen, N. L. (1928). The evolution of igneous rocks. *Science Progress, (1894–1898)*, *1*(2), 152–165.

Chappell, B. W., & White, A. J. R. (1974). Two contrasting granite types. *Pacific Geology*, *8*(2), 173–174.

Chappell, B. W., White, A. J. R., Williams, I. S., Wyborn, D., & Wyborn, L. A. I. (2000). Lachlan Fold Belt granites revisited: High- and low-temperature granites and their implications. *Australian Journal of Earth Sciences*, *47*, 123–138. https://doi.org/10.1046/j.1440-0952.2000.00766.x

Chauvel, C., Lewin, E., Carpentier, M., Arndt, N. T., & Marini, J. C. (2008). Role of recycled oceanic basalt and sediment in generating the Hf–Nd mantle array. *Nature Geoscience*, *1*, 64–67. https://doi.org/10.1038/ngeo.2007.51

Chen, S., Niu, Y., Li, J., Sun, W., Zhang, Y., & Hu, Y. (2016). Syn-collisional adakitic granodiorites formed by fractional crystallization: Insights from their enclosed mafic magmatic enclaves (mmes) in the Qumushan pluton, North Qilian Orogen at the northern margin of the Tibetan Plateau. *Lithos*, *248–251*, 455–468.

Chen, S., Niu, Y. L., Sun, W. L., Zhang, Y., Li, J. Y., Guo, P. Y., & Sun, P. (2015). On the origin of mafic magmatic enclaves (MMEs) in syn-collisional granitoids: Evidence from the Baojishan pluton in the North Qilian Orogen, China. *Mineralogy and Petrology*, *109*(5), 577–596. https://doi.org/10.1007/s00710-015-0383-5

Collins, W. J., Beams, S. D., White, A. J. R., & Chappell, B. W. (1982). Nature and origin of A-type granites with particular reference to south-eastern Australia. *Contributions to Mineralogy and Petrology*, *80*(2), 189–200.

Condie, K. C. (2000). Episodic continental growth models: Afterthoughts and extensions. *Tectonophysics*, *322*, 153–162. https://doi.org/10.1016/S0040-1951(00)00061-5

Corfu, F., Hanchar, J. M., Hoskin, P. W. O., & Kinny, P. (2003). Altas of zircon textures. *Reviews in Mineralogy and Geochemistry*, *53*, 469–500. https://doi.org/10.2113/0530469

Depaolo, D. J. (1981). Trace element and isotopic effects of combined wallrock assimilation and fractional crystallization. *Earth and Planetary Science Letters*, *53*(2), 189–202. https://doi.org/10.1016/0012-821X(81)90153-9

Dong, Y., Liu, X., Zhang, G., Chen, Q., Zhang, X., Li, W., & Yang, C. (2012). Triassic diorites and granitoids in the Foping area: Constraints on the conversion from subduction to collision in the Qinling orogen, China. *Journal of Asian Earth Sciences*, *47*, 123–142. https://doi.org/10.1016/j.jseaes.2011.06.005

Dong, Y., Zhang, X., Liu, X., Li, W., Chen, Q., Zhang, G., & Zhang, F. (2015). Propagation tectonics and multiple accretionary processes of the Qinling Orogen. *Journal of Asian Earth Sciences*, *104*, 84–98. https://doi.org/10.1016/j.jseaes.2014.10.007

Dong, Y. P., Zhang, G. W., Neubauer, F., Liu, X. M., Genser, J., & Hauzenberger, C. (2011). Tectonic evolution of the Qinling orogen, China: Review and synthesis. *Journal of Asian Earth Sciences*, *41*, 213–237. https://doi.org/10.1016/j.jseaes.2011.03.002

Duan, M., Niu, Y. L., Kong, J. J., Zhang, Y., Hu, Y., & Sun, P. (2016). Zircon U–Pb geochronology, Sr–Nd–Hf isotopic geochemistry and geological significance of Baijiazhuang and Lvjing granitic plutons in West Qinling Orogen. *Lithos*, *260*, 443–456. https://doi.org/10.1016/j.lithos.2016.04.015

Eberz, G. W., & Nicholls, I. A. (1990). Chemical modification of enclave magma by post-emplacement crystal fractionation, diffusion and metasomatism. *Contributions to Mineralogy and Petrology*, *104*(1), 47–55. https://doi.org/10.1007/BF00310645

Elburg, M. A. (1996). Evidence of isotopic equilibration between microgranitoid enclaves and host granodiorite, Warburton Granodiorite, Lachlan Fold Belt, Australia. *Lithos*, *38*, 1–22. https://doi.org/10.1016/0024-4937(96)00003-5

Ewart, A., & Griffin, W. L. (1994). Application of proton-microprobe data to trace-element partitioning in volcanic-rocks. *Chemical Geology*, *117*(1–4), 251–284. https://doi.org/10.1016/0009-2541(94)90131-7

Feng, Y. M., Cao, X. Z., Zhang, E. P., Hu, Y. X., Pan, X. P., Yang, J. L., … Li, W. M. (2002). *Structure, orogenic processes and geodynamic of the western Qinling orogen (in Chinese)* (pp. 1–263). Xi'an: Xi'an Map Press.

Foley, S., Tiepolo, M., & Vannucci, R. (2002). Growth of early continental crust controlled by melting of amphibolite in subduction zones. *Nature*, *417*, 837–840. https://doi.org/10.1038/nature00799

Gao, S., Rudnick, R. L., Yuan, H. L., Liu, X. M., Liu, Y. S., Xu, W. L., … Wang, Q. H. (2004). Recycling lower continental crust in the North China craton. *Nature*, *432*, 892–897. https://doi.org/10.1038/nature03162

Gao, T. (2011). *The LA-ICP-MS zircon U–Pb dating, geology and geochemistry, tectonic setting of several important intrusions from the north part of the western stage of west Qinling and their relationship with mineralization* (doctoral dissertation).

Griffin, W. L., Wang, X., Jackson, S. E., Pearson, N. J., O'Reilly, S. Y., Xu, X. S., & Zhou, X. M. (2002). Zircon chemistry and magma mixing, SE China: In-situ analysis of Hf isotopes, Tonglu and Pingtan igneous complexes. *Lithos*, *61*(3), 237–269. https://doi.org/10.1016/S0024-4937(02)00082-8

Hanchar, J. M., & Hoskin, P. W. O. (2003). Zircon. *Reviews in Mineralogy and Geochemistry*, *53*, 1–500.

Holden, P., Halliday, A. N., & Stephens, W. E. (1987). Neodymium and strontium isotope content of microdiorite enclaves points to mantle input to granitoid production. *Nature*, *330*(6143), 53–56. https://doi.org/10.1038/330053a0

Huang, H., Niu, Y. L., Nowell, G., Zhao, Z. D., Yu, X. H., Zhu, D. C., … Ding, S. (2014). Geochemical constraints on the petrogenesis of granitoids in the East Kunlun Orogenic belt, northern Tibetan Plateau: Implications for continental crust growth through syn-collisional felsic magmatism. *Chemical Geology*, *370*, 1–18. https://doi.org/10.1016/j.chemgeo.2014.01.010

Jahn, B. M., Wu, F. Y., & Chen, B. (2000). Massive granitoid generation in central Asia: Nd isotopic evidence and implication for continental growth in the Phanerozoic. *Episodes*, *23*, 82–92.

Jiang, H. (2016). *Granite magmatism and tectonic setting of "Five Golden Flower" granite plutons in Lixian-Minxian ore concentrated area, Western Qinling*. Northwest University, master's thesis.

Jiang, Y. H., Jin, G. D., Liao, S. Y., Zhou, Q., & Zhao, P. (2010). Geochemical and Sr–Nd–Hf isotopic constraints on the origin of Late Triassic granitoids from the Qinling orogen, central China: Implications for a continental arc to continent-continent collision. *Lithos*, *117*(1–4), 183–197. https://doi.org/10.1016/j.lithos.2010.02.014

Kong, J. J., Niu, Y. L., Duan, M., Zhang, Y., Hu, Y., Li, J. Y., & Chen, S. (2017). Petrogenesis of Luchuba and Wuchaba granitoids in western Qinling: Geochronological and geochemical evidence. *Mineralogy and Petrology*, *111*, 887–908. https://doi.org/10.1007/s00710-017-0501-7

Lai, S. C., & Zhang, G. W. (1996). Geochemical features of ophiolites in Mianxian-Lueyang suture zone, Qinling Orogenic Belt. *Journal of China University of Geosciences*, *7*, 165–172.

Leake, B. E., Woolley, A. R., Arps, C. E. S., Birch, W. D., Gilbert, M. C., Grice, J. D. (1997). Nomenclature of amphiboles; Report of the Subcommittee on Amphiboles of the International Mineralogical Association, Commission on New Minerals and Mineral Names. International Conference on Formal Concept Analysis, 4390, 181–196.

Lee, C. T. A., & Anderson, D. L. (2015). Continental crust formation at arcs, the arclogite "delamination" cycle, and one origin for fertile melting anomalies in the mantle. *Science Bulletin*, *60*(13), 1141–1156. https://doi.org/10.1007/s11434-015-0828-6

Li, X. H., Li, Z. X., Li, W. X., Liu, Y., Yuan, C., Wei, G. J., & Qi, C. S. (2007). U–Pb zircon, geochemical and Sr–Nd–Hf isotopic constraints on age and origin of Jurassic I- and A-type granites from central Guangdong, SE China: A major igneous event in response to foundering of a subducted flat-slab? *Lithos*, *96*, 186–204. https://doi.org/10.1016/j.lithos.2006.09.018

Li, Y., Liang, W., Zhang, G., Jiang, D., & Wang, J. (2017). Tectonic setting of the late Triassic magmatism in the Qinling orogen: New constraints from the interplay between granite emplacement and shear zone deformation in the shagou area. *Geological Journal*, *52*(S1), 250–271. https://doi.org/10.1002/gj.3068

Li, Y. J., Duan, Y. M., & Li, X. F. (1993). Internal contact relationship and geological mapping of super unit and unit system for granites in the Taoping Region of the western Qinling. *Journal of Xi'an College of Geology*, *15*, 98–106.

Liang, W., Zhang, G., Bai, Y., Jin, C., & Nantasin, P. (2015). New insights into the emplacement mechanism of the Late Triassic granite plutons in the Qinling orogen: A structural study of the Mishuling pluton. *Geological Society of America Bulletin*, *127*(11–12), 1583–1603. https://doi.org/10.1130/B31187.1

Lin, W. W., & Peng, L. J. (1994). The estimation of Fe^{3+} and Fe^{2+} contents in amphibole and biotite from EMPA data. *Journal of Changchun University Earth Sciences*, *24*, 155–162. (in Chinese with English abstract).

Liu, F. L., Xu, Z. Q., Liou, J. G., & Song, B. (2004). SHRIMP U–Pb ages of ultrahigh-pressure and retrograde metamorphism of gneisses, southwestern Sulu terrane, eastern China. *Journal of Metamorphic Geology*, *22*, 315–326. https://doi.org/10.1111/j.1525-1314.2004.00516.x

Liu, S. W., Li, Q. G., Tian, W., Wang, Z. Q., Yang, P. T., Wang, W., … Guo, R. R. (2011). Petrogenesis of Indosinian granitoids in Middle-Segment of South Qinling Tectonic Belt: Constraints from Sr–Nd isotopic systematics. *Acta Geologica Sinica-English Edition*, *85*, 610–628. https://doi.org/10.1111/j.1755-6724.2011.00455.x

Liu, S. W., Yang, P. T., Li, Q. G., Wang, Z. Q., Zhang, W. Y., & Wang, W. (2011). Indosinian granitoids and orogenic processes in the middle segment of the Qinling orogen, China. *Journal of Jilin University (Earth Science Edition)*, *41*(6).

Ludwig, K. (2012). *User's manual for Isoplot version 3.75–4.15: A geochronological toolkit for Microsoft*Excel Berkley Geochronological Center Special Publication, No. 5.

Mattauer, M., Matte, P., Malavieille, J., Tapponnier, P., Maluski, H., Qin, X. Z., & Qin, T. Y. (1985). Tectonics of the Qinling belt: Build-up and evolution of eastern Asia. *Nature*, *317*, 496–500. https://doi.org/10.1038/317496a0

Meng, Q. R., & Zhang, G. W. (2000). Geologic framework and tectonic evolution of the Qinling-Dabie orogen, central China. *Tectonophysics*, *323*, 183–196. https://doi.org/10.1016/S0040-1951(00)00106-2

Mo, X. X., Niu, Y. L., Dong, G. C., Zhao, Z. D., Hou, Z. Q., Zhou, S., & Ke, S. (2008). Contribution of syncollisional felsic magmatism to continental crust growth: A case study of the Paleogene Linzizong volcanic succession in southern Tibet. *Chemical Geology*, *250*, 49–67. https://doi.org/10.1016/j.chemgeo.2008.02.003

Niu, Y. L. (2017). Slab breakoff: A causal mechanism or pure convenience? *Science Bulletin*, *62*, 456–461. https://doi.org/10.1016/j.scib.2017.03.015

Niu, Y.L., Mo, X.X., Dong, G.C., Zhao, Z.D., Hou, Z.Q., Zhou, S., Ke, S. (2007). Continental collision zones are primary sites of net continental crustal growth: Evidence from the Linzizong volcanic succession in southern Tibet. Eos Trans. AGU, 88(52), Fall Meet., Suppl., Abstract 34, 01.

Niu, Y. L., & O'Hara, M. J. (2009). MORB mantle hosts the missing Eu (Sr, Nb, Ta and Ti) in the continental crust: New perspectives on crustal growth, crust-mantle differentiation and chemical structure of oceanic upper mantle. *Lithos*, *112*, 1–17. https://doi.org/10.1016/j.lithos.2008.12.009

Niu, Y. L., Zhao, Z. D., Zhu, D. C., & Mo, X. X. (2013). Continental collision zones are primary sites for net continental crust growth-A testable hypothesis. *Earth-Science Reviews*, *127*, 96–110. https://doi.org/10.1016/j.earscirev.2013.09.004

Pearce, J. A., & Peate, D. W. (1995). Tectonic implications of the composition of volcanic arc magmas. *Annual Review of Earth and Planetary Sciences*, *23*, 251–286. https://doi.org/10.1146/annurev.ea.23.050195.001343

Peng, X. (2013). Research on homology for the rock group of monzonite granite in the western Qinling. *Northwestern Geology*, *46*, 63–80.

Pin, C., Binon, M., Belin, J. M., Barbarin, B., & Clemens, J. D. (1990). Origin of microgranular enclaves in granitoids: Equivocal Sr–Nd evidence from Hercynian rocks in the massif central (France). *Journal of Geophysical Research Solid Earth*, *95*(B11), 17821–17828. https://doi.org/10.1029/JB095iB11p17821

Poli, G. E., & Tommasini, S. (1991). Model for the origin and significance of microgranular enclaves in calc-alkaline granitoids. *Journal of Petrology*, *32*(3), 657–666. https://doi.org/10.1093/petrology/32.3.657

Qin, J. F., Lai, S. C., Grapes, R., Diwu, C. R., Ju, Y. J., & Li, Y. F. (2009). Geochemical evidence for origin of magma mixing for the Triassic monzonitic granite and its enclaves at Mishuling in the Qinling orogen (central China). *Lithos*, *112*, 259–276. https://doi.org/10.1016/j.lithos.2009.03.007

Qin, J. F., Lai, S. C., Grapes, R., Diwu, C. R., Ju, Y. J., & Li, Y. F. (2010). Origin of Late Triassic high Mg adakitic granitoid rocks from the Dongjiangkou area, Qinling orogen, central China implications for subduction of continental crust. *Lithos*, *120*, 347–367. https://doi.org/10.1016/j.lithos.2010.08.022

Ratschbacher, L., Hacker, B. R., Calvert, A., Webb, L. E., Crimmer, J. C., McWilliams, M. O., … Hu, J. (2003). Tectonics of the Qinling (Central China): Tectonostratigraphy, geochronology, and deformation history. *Tectonophysics*, *366*, 1–53. https://doi.org/10.1016/S0040-1951(03)00053-2

Reid, J. B. Jr., & Hamilton, M. A. (1987). Origin of Sierra Nevadan granite: Evidence from small scale composite dikes. *Contrib Mineral Petrol*, *96*, 441–454.

Reiners, P. W., Nelson, B. K., & Ghiorso, M. S. (1995). Assimilation of felsic crust by basaltic magma: Thermal limits and extents of crustal contamination of mantle-derived magmas. *Geology*, *23*(6), 563. https://doi.org/10.1130/0091-7613(1995)023<0563:AOFCBB>2.3.CO;2

Reiners, P. W., Nelson, B. K., & Nelson, S. W. (1996). Evidence for multiple mechanisms of crustal contamination of magma from compositionally zoned plutons and associated ultramafic intrusions of the Alaska Range. *Journal of Petrology*, *37*(2), 261–292. https://doi.org/10.1093/petrology/37.2.261

Rollison, H. (1993). *Using geochemical data: Evaluation, presentation, interpretation* (Vol. 352). London: Longman Scientific and Technical.

Rubatto, D., & Gebauer, D. (2000). Use of cathodoluminescence for U–Pb zircon dating by ion microprobe: Some examples from the Western Alps. In *Cathodoluminescence in geosciences* (pp. 373–400). Berlin: Springer. https://doi.org/10.1007/978-3-662-04086-7_15

Rudnick, R. L., Gao, S. (2003). Composition of the continental crust. *Treatise on geochemistry*, 3, 1–64, https://doi.org/10.1016/B0-08-043751-6/03016-4

Shao, F. L., Niu, Y. L., Liu, Y., Chen, S., Kong, J. J., & Duan, M. (2017). Petrogenesis of Triassic granitoids in the East Kunlun Orogenic Belt, northern Tibetan Plateau and their tectonic implications. *Lithos*, *282-283*, 33–44. https://doi.org/10.1016/j.lithos.2017.03.002

Shen, J., Zhang, Z. Q., & Liu, D. Y. (1997). Sm–Nd, Rb–Sr, $^{40}Ar/^{39}Ar$, $^{207}Pb/^{206}Pb$ age of the Douling metamorphic complex from eastern Qinling orogenic belt. *Acta Geoscientia Sinica*, *18*(3), 248–254.

Song, S., Niu, Y., Wei, C., Ji, J., & Su, L. (2010). Metamorphism, anatexis, zircon ages and tectonic evolution of the Gongshan block in the northern Indochina continent—An eastern extension of the Lhasa Block. *Lithos*, *120*(3), 327–346. https://doi.org/10.1016/j.lithos.2010.08.021

Song, S. G., Su, L., Li, X. H., Zhang, G. B., Niu, Y. L., & Zhang, L. F. (2010). Tracing the 850-Ma continental flood basalts from a piece of subducted continental crust in the North Qaidam UHPM belt, NW China. *Precambrian Research*, *183*, 805–816. https://doi.org/10.1016/j.precamres.2010.09.008

Sun, S., & McDonough, W. F. (1989). Chemical and isotopic systematics of oceanic basalts: Implications for mantle composition and processes. *Geological Society*, *London*, *Special Publications*, *42*, 313–345. https://doi.org/10.1144/GSL.SP.1989.042.01.19

Sun, W. D., Li, S. G., Chen, Y. D., & Li, Y. J. (2002). Timing of synorogenic granitoids in the South Qinling, central China: Constraints on the evolution of the Qinling-Dabie orogenic belt. *Journal of Geology*, *110*, 457–468. https://doi.org/10.1086/340632

Sun, P., Niu, Y., Guo, P., Chen, S., Duan, M., Gong, H., … Xiao, Y. (2018). Multiple mantle metasomatism beneath the Leizhou Peninsula, South China: Evidence from elemental and Sr-Nd-Pb-Hf isotope geochemistry of the late Cenozoic volcanic rock (in preparation).

Taylor, S. R. (1967). The origin and growth of continents. *Tectonophysics*, *4*, 17–34. https://doi.org/10.1016/0040-1951(67)90056-X

Vervoort, J. D., Patchett, P. J., Blichert-Toft, J., & Albarède, F. (1999). Relationships between Lu–Hf and Sm–Nd isotopic systems in the global sedimentary system. *Earth and Planetary Science Letters*, *168*, 79–99. https://doi.org/10.1016/S0012-821X(99)00047-3

Vervoort, J. D., Plank, T., & Prytulak, J. (2011). The Hf–Nd isotopic composition of marine sediments. *Geochimica et Cosmochimica Acta*, *75*, 5903–5926. https://doi.org/10.1016/j.gca.2011.07.046

Wang, Z. Q., Yan, Q. R., Yan, Z., Wang, T., Jiang, C. F., Gao, L. D., & Liu, P. (2009). The new division of the main tectonic unit for the Qinling orogenic belt. *Journal of Geology*, *3*(11), 1527–1546.

Wen, Z. L. (2008). A new recognition of magma mixing process about jiaochangba rock body, Western Qinling. *Journal of Mineralogy and Petrology*, *3*, 29–36.

Whalen, J. B. (1985). Geochemistry of an island-arc plutonic suite: The Uasilau-Yau Yau intrusive complex, New Britain P.N.G. *Journal of Petrology*, *26*, 603–632. https://doi.org/10.1093/petrology/26.3.603

Wiedenbeck, M., Alle, P., Corfu, F., Griffin, W. L., Meier, M., Oberli, F., … Speigel, W. (1995). Three natural zircon standards for U–Th–Pb, Lu–Hf, trace-element and REE analyses. *Geostandards Newsletter*, *19*, 1–23. https://doi.org/10.1111/j.1751-908X.1995.tb00147.x

Wu, Y. B., & Zheng, Y. F. (2012). Tectonic evolution of a composite collision orogen: An overview on the Qinling-Tongbai-Hong'an-Dabie-Sulu orogenic belt in central China. *Gondwana Research*, *23*, 1402–1428.

Xiao, B., Li, Q., Liu, S., Wang, Z., Yang, P., Chen, J., & Xu, X. (2014). Highly fractionated Late Triassic I-type granites and related molybdenum mineralization in the Qinling orogenic belt: Geochemical and U–Pb–Hf and Re–Os isotope constraints. *Ore Geology Reviews*, *56*, 220–233. https://doi.org/10.1016/j.oregeorev.2013.07.003

Xiao, L. (2004). *Geological map of Minxian and Tianshui: Chinese geological survey*, *scale 1: 250,000*, *2 sheets*.

Xu, J. F., Castillo, P. R., Li, X. H., Zhang, B. R., & Han, Y. W. (2002). MORB-type rocks from the Paleo-Tethyan Mian-Lueyang northern ophiolite in the Qinling Mountains, central China: Implications for the source of the low $^{206}Pb/^{204}Pb$ and high $^{143}Nd/^{144}Nd$ mantle component in the Indian ocean. *Earth and Planetary Science Letters*, *198*, 323–337. https://doi.org/10.1016/S0012-821X(02)00536-8

Xu, Y. L., M, Y. Z., & Wang, G. G. (2006). Discusson diagenetic and metallogenic features and metallogenic Mechanism of Bojiazhuang rock mass in Minxian-Lixian area of Gansu province. *Gansu Geology*, *15*, 126–132.

Yan, Z., Wang, Z., Li, J., Xu, Z., & Deng, J. (2012). Tectonic settings and accretionary orogenesis of the West Qinling Terrane, northeastern margin of the Tibet Plateau. *Acta Petrologica Sinica*, *28*, 1808–1828.

Yang, J. S., Wu, F. Y., Wilde, S., & Liu, X. (2007). Petrogenesis of late Triassic granitoids and their enclaves with implications for post-collisional lithospheric thinning of the Liaodong Peninsula, North China Craton. *Chemical Geology*, *242*, 155–175. https://doi.org/10.1016/j.chemgeo.2007.03.007

Yang, P. T., Liu, S. W., Li, Q. G., Wang, Z. Q., Wang, R. T., & Wang, W. (2012). Geochemistry and zircon U–Pb–Hf isotopic systematics of the Ningshan granitoid batholith, middle segment of the South Qinling belt, Central China: Constraints on petrogenesis and geodynamic processes. *Journal of Asian Earth Sciences*, *61*, 166–186. https://doi.org/10.1016/j.jseaes.2012.09.013

Yang, P. T., Liu, S. W., Li, Q. G., Zhang, F., Wang, Z. Q., Wang, D. S., … Yan, Z. (2011). Ages of the Laocheng granitoids and crustal growth in the South Qinling Tectonic Domain, Central China: Zircon U–Pb and Lu–Hf isotopic constraints. *Acta Geologica Sinica-English Edition*, *85*, 854–869. https://doi.org/10.1111/j.1755-6724.2011.00490.x

Yang, S. S., Liu, J. J., Zhang, F., Yuan, F., Zhai, D. G., & Li, Y. J. (2017). Petrogenesis and geodynamic setting of the Triassic granitoid plutons in West Qinling, China: Insights from LA-ICP-MS zircon U–Pb ages, Lu–Hf isotope signatures and geochemical characteristics of the Zhongchuan pluton. *Intenational Geology Review*, *2*, 1–21.

Yang, Y., Wang, X. X., Ke, C. H., Wang, S. A., Li, J. B., Nie, Z. R., & Lv, X. Q. (2015). Zircon U–Pb ages and petrogenesis of the Luchuba pluton in West Qinling, and its geological significance. *Acta Geologica Sinica*, *89*, 1735–1761.

Yang, Y. H., Zhang, H. F., Chu, Z. Y., Xie, L. W., & Wu, F. Y. (2010). Combined chemical separation of Lu, Hf, Rb, Sr, Sm and Nd from a single rock digest and precise and accurate isotope determinations of Lu–Hf, Rb–Sr and Sm–Nd isotope systems using Multi-Collector ICP-MS and TIMS. *International Journal of Mass Spectrometry*, *290*, 120–126. https://doi.org/10.1016/j.ijms.2009.12.011

Yuan, H. L., Fuyuan, W. U., Shan, G., Liu, X., Ping, X. U., & Sun, D. (2003). Determination of U–Pb age and rare earth element concentrations of zircons from Cenozoic intrusions in northeastern China by laser ablation ICP-MS. *Science Bulletin*, *48*, 2411–2421.

Zhang, C. L., Zhang, G. W., Yan, Y. X., & Wang, Y. (2005). Origin and dynamic significance of Guangtoushan granitic plutons to the north of Mianlue zone in southern Qinling. *Acta Petrologica Sinca*, *21*, 711–720.

Zhang, G. W., Zhang, B. R., Yuan, X. C., & Xiao, Q. H. (2001). *Qinling Orogen Belt and continental geodynamics* (pp. 1–729). Beijing: Science Press.

Zhang, H., Jin, L., Zhang, L., Nigel, H., Zhou, L., Hu, S., & Zhang, B. (2007). Geochemical and Pb–Sr–Nd isotopic compositions of granitoids from western Qinling belt: Constraints on basement nature and tectonic affinity. *Science in China Series D: Earth Sciences*, *50*, 184–196. https://doi.org/10.1007/s11430-007-2015-3

Zhang, Y., Niu, Y. L., Hu, Y., Liu, J. J., Ye, L., Kong, J. J., & Duan, M. (2016). The syncollisional granitoid magmatism and continental crustal growth in the West Kunlun Orogen, China—Evidence from geochronology and geochemistry of the Arkarz pluton. *Lithos*, *245*, 191–204.

Zhang, Z. Q., Zhang, G. W., & Tang, S. H. (2002). *Isotopic chronology of south Qinling metamorphic rock-group* (pp. 1–256). Beijing: Geological Publishing House.

Zheng, Y. F. (2008). A perspective view on ultrahigh-pressure metamorphism and continental collision in the Dabie-Sulu orogenic belt. *Chinese Science Bulletin*, *53*, 3081–3104.

Zhong, H., Zhu, W. G., Hu, R. Z., Xie, L. W., He, D. F., Liu, F., & Chu, Z. Y. (2009). Zircon U–Pb age and Sr–Nd–Hf isotope geochemistry of the Panzhihua A-type syenitic intrusion in the Emeishan large igneous province, southwest China and implications for growth of juvenile crust. *Lithos*, *110*, 109–128. https://doi.org/10.1016/j.lithos.2008.12.006

Zhu, L., Zhang, G., Yang, T., Wang, F., & Gong, H. (2013). Geochronology, petrogenesis and tectonic implications of the Zhongchuan granitic pluton in the Western Qinling metallogenic belt, China. *Geological Journal*, *48*, 310–334. https://doi.org/10.1002/gj.2444

Zhu, L. M., Zhang, G. W., Chen, Y. J., Ding, Z. J., Guo, B., Wang, F., & Lee, B. (2011). Zircon U–Pb ages and geochemistry of the Wenquan Mo-bearing granitoids in West Qinling, China: Constraints on the geodynamic setting for the newly discovered Wenquan Mo deposit. *Ore Geology Reviews*, *39*, 46–62. https://doi.org/10.1016/j.oregeorev.2010.10.001

How to cite this article: Kong J, Niu Y, Duan M, et al. The syncollisional granitoid magmatism and crust growth during the West Qinling Orogeny, China: Insights from the Jiaochangba pluton. *Geological Journal*. 2019;54:4014–4033. https://doi.org/10.1002/gj.3368

APPENDIX A
THE Sr-Nd-Hf ISOTOPES REPLICATE ANALYSES RESULTS OF THE INTERNATIONAL REFERENCE MATERIALS

Sample	$^{87}Sr/^{86}Sr$	¡À2¦Ò	$^{143}Nd/^{144}Nd$	¡À2¦Ò	$^{176}Hf/^{177}Hf$	¡À2¦Ò
AGV-2	0.704196	0.000004	0.512785	0.000003	0.282977	0.000002
GSP-2	0.71025	0.000004	0.511369	0.000003	0.283012	0.000002
RGM-2	0.76521	0.000004	0.512803	0.000003	0.282554	0.000002